Research Article

Projectile Excitation to the 2s2p ^{3}P and ^{1}P Autoionizing States in Swift Collisions of He-Like Carbon and Oxygen Mixed-State (1s^2, 1s2s ^{3}S) Ion Beams With Helium

Angelos Laoutaris[1,2], Stylianos Passalidis[3], Stefanos Nanos[2,4,5], Emmanouil (Manolis) P. Benis[4], Alain Dubois[3], Theo Zouros[1]

1. Department of Physics, University of Crete, Greece; 2. Tandem Accelerator Laboratory, Institute of Nuclear and Particle Physics, NCSR "Demokritos", Greece; 3. Laboratoire de Chimie Physique – Matière et Rayonnement, Sorbonne Université, France; 4. Department of Physics, University of Ioannina, Greece; 5. Department of Physics (Present), University of Crete, Greece

The production of the projectile $2s2p\,^3P$ and $2s2p\,^1P$ autoionizing states is investigated in 0.5-1.5 MeV/u collisions of He-like carbon and oxygen mixed-state three-component $(1s^2, 1s2s\,^3S, 1s2s\,^1S)$ ion beams with helium targets. The mixed-state beams are produced in the stripping systems of the 5.5 MV Demokritos tandem accelerator. Using high-resolution Auger projectile electron spectroscopy, the normalized Auger electron yields are measured at 0° relative to the beam direction. In addition, a three-electron atomic orbital close-coupling approach, employing full configuration interaction and antisymmetrization of the three-electron, two-center total wave function, is applied to calculate the production cross sections for these states from each of the three initial ion beam components. Thereupon, the theoretical Auger yields are computed and found to be smaller than experiment by factors ranging from about 1.2 to 7.6. Agreement, however, improves when larger $1s2s\,^1S$ fractions, not only based on spin statistics, are projected. Overall, this non-perturbative treatment of excitation, which does not rely on scaling parameters or renormalization, marks a significant advancement in the modeling of multielectron, multi-open-shell quantum systems subjected to ultrafast perturbations, where current understanding remains incomplete.

Corresponding author: T. J. M. Zouros, tzouros@physics.uoc.gr

I. Introduction

The excitation of an electron from one bound state to another is a fundamental quantum mechanical process and together with electron capture and ionization constitutes one of the most important ion-atom collision processes. Recently, we investigated $1s \rightarrow 2p$ projectile excitation, both experimentally and theoretically, in the production of $2s2p\,^3P$ states from initial $1s2s\,^3S$ metastable states in energetic (MeV/u) collisions of He-like carbon and oxygen

 doi.org/10.32388/C8JRSC

ions with helium[1]. Here, in a more comprehensive treatment, we extend these investigations to also include the production of the $2s2p\,^1P$ states from the $1s^2$ ground state, as well as from both $1s2s\,^3S$ and $1s2s\,^1S$ metastable states, all three initial states naturally found in He-like ion beams. Excitation from such pre-excited initial states presents a real challenge to the modeling of such multielectron multi-open-shell dynamical quantum systems.

High-energy two-electron projectile ions colliding with targets represent a unique three-electron collision system for investigating few-electron quantum dynamics[2]. Such three-electron systems, while simple enough to allow for the identification of individual excitation processes and the calculation of their cross sections, are also complex enough to present a real challenge to *ab initio* non-perturbative theoretical approaches[3]. Important applications include solar flares[4], calibration of existing and developing new X-ray line diagnostics[5], high temperature fusion and astrophysical plasmas[6], as well as fusion plasma heating and diagnostics[7].

Swift (MeV/u), He-like ion beams provided by accelerators can deliver such two-electron projectiles. Tandem Van de Graaff accelerators, in particular, use their intrinsic beam up-charging stripper systems[8] to generate such highly-charged, low-Z_p atomic number beams allowing for collision energy E_p - and isoelectronic Z_p -dependent studies that reveal intriguing and important systematic features of the collision dynamics[9].

The stripping process, in the case of such energetic He-like ion beams, gives rise not only to the $1s^2$ ground state, but also to the long-lived $1s2s\,^3S$ (for short ^3S) and $1s2s\,^1S$ (for short ^1S) states. The lifetimes of such first-row ion metastable states are in the range of $10^{-3} - 10^{-7}$ s[9] and therefore long enough to survive to the target.

This admixture of metastable states is particularly rich in atomic physics information as it provides *unique* access to both singly- and doubly-excited states otherwise inaccessible from just a *pure* ground state beam[9]. However, it presents the additional difficulty of having to accurately determine its fractional composition since production cross sections from these pre-excited states can be much larger than from the ground state. This knowledge is essential for precise quantitative comparisons between theory and experiment.

For the $1s2s\,^3S$ state, various measurement techniques have been used to date, indicating that for first-row atoms a significant fraction in the ^3S state, $f[^3S] \sim 10 - 30\%$[10][11][12][13][14][15][16] survives to the target. However, for the ^1S state - having a much shorter lifetime - the corresponding fraction is smaller and has never been directly measured. Instead, its estimation, at $f[^1S] \sim 0.1 - 3\%$[12] has been based on various stripper production models[8][12][14][15][16][17], mostly assuming it is produced in a 1:3 spin statistics ratio relative to the measured $f[^3S]$ fraction.

Recently, there has been renewed interest in using mixed-state He-like ion beams in collisions with helium, driven by advancements in state-selective, *ab initio*, non-perturbative close-coupling calculations[3]. In particular, semi-classical three-electron atomic orbital close-coupling (3eAOCC) calculations, involving mixed-state He-like carbon and oxygen ions, have provided state-selective cross sections for processes such as single electron capture (SEC)[18][19], transfer excitation (TE)[20], and projectile excitation[1], enhancing our understanding of multi-electronic interactions in multi-open-shell quantum systems under intense, ultrafast perturbations.

For low-Z_p He-like ions, the production of doubly-excited autoionizing states has been effectively studied using Auger projectile spectroscopy. Zero-degree Auger projectile spectroscopy (ZAPS)[21][22], which detects emitted Auger electrons at $\theta = 0^\circ$ relative to the beam direction, has been particularly successful in providing state-selective production cross sections. These measurements offer well-defined initial and final states, thereby providing stringent tests of theory. An important advantage in using ZAPS is that the $1s2s\,^3S$ metastable fraction can be measured directly from the Auger spectra themselves: First, using a two-component approach[14][15][17][23], where the ^1S fraction was neglected, and very recently in a full three-component approach, which included the ^1S fraction using a new model, providing a self-consistent three-component fractional determination[8].

Thus, using ZAPS to provide state selective measurements and an accurate *in situ* technique to measure the fractional components combined with state-of-the art 3eAOCC calculations to provide state production cross sections from each of the three components has been particularly productive. In particular, investigations of SEC in carbon resolved a long-standing spin-statistics problem[18][19]. Investigations of TE provided the first coherent treatment of dynamic electron-electron correlations, successfully describing resonance transfer-excitation (RTE) and revealed a new low-energy nonresonant one-step transfer-excitation mechanism[20]. Investigations of cusp-electron production using mixed-state He-like oxygen ion beams showed the ^3S component to play an important role which could be quantitatively well-described by continuous-distorted-wave theories of electron-loss and electron-capture to the continuum[24]. Very recently, investigations of $1s \rightarrow 2p$ excitation[1] in the production of $2s2p\,^3P$ states from just the $1s2s\,^3S$ state in collisions of carbon and oxygen ions with helium indicate that the conventional first Born picture of screening and antiscreening mechanisms might need revision.

Here, we further pursue single and double excitation including the production of both $2s2p\,^3P$ and $2s2p\,^1P$ states from all three initial ion beam components:

$$\mathrm{Z}^{q+}(1s2s\,^3S) + \mathrm{He} \rightarrow \mathrm{Z}^{q+}(2s2p\,^{3,1}P) + \mathrm{He(All)}, \quad (1)$$
$$\mathrm{Z}^{q+}(1s2s\,^1S) + \mathrm{He} \rightarrow \mathrm{Z}^{q+}(2s2p\,^{3,1}P) + \mathrm{He(All)}, \quad (2)$$
$$\mathrm{Z}^{q+}(1s^2\,^1S) + \mathrm{He} \rightarrow \mathrm{Z}^{q+}(2s2p\,^{3,1}P) + \mathrm{He(All)}, \quad (3)$$
$$\lfloor\!\rightarrow \mathrm{Z}^{(q+1)+}(1s) + e_A^-(0^\circ), \quad (4)$$

with the emitted Auger electrons, e_A^-, from the decay of the two $2s2p$ states (4) detected at the laboratory observation angle of $\theta = 0^\circ$ relative to the ion beam using ZAPS. Normalized Auger yields are measured in the collision energy range of 0.5-1.5 MeV/u, where Z^{q+} denotes C^{4+} or O^{6+} ion projectiles. He(All), indicates that all resulting final helium target states, from processes including simultaneous target single excitation and ionization are considered in the calculations, since the final states of the target were not experimentally determined. Accompanying 3eAOCC calculations within a full configuration interaction approach provide the production cross sections. Thus, cross sections for both *single* direct and exchange $1s \rightarrow 2p$ excitation [Eqs. (1)-(2)] and similarly for *double* $(1s \rightarrow 2s, 1s \rightarrow 2p)$ excitation [Eq. (3) direct for ^1P and exchange for ^3P] are reported.

Historically, over the past 50 years, there has been much interest in the excitation of atoms or ions in atomic collisions, as well as related work on electron impact excitation and photo-excitation. Generic references were already given in Ref.[1].

Early high-resolution x-ray studies using He-like ions[25][26][27][28][29][30][31][32][33][34][35] largely focused on the production of singly-excited $1s2p\,^3P$ and $1s2p\,^1P$ states. However, these measurements were often complicated by cascade effects[26][36][37], which made interpretation challenging. Subsequent research examined doubly-excited states through high-resolution Auger spectroscopy[11][38], which are less affected by cascades due to low radiative branching ratios in first-row atoms. Notably, the first report on $2s2p\,^3P$ production from the ^3S state in energetic mixed-state F^{7+} ions colliding with He and H_2—compared to first Born cross-section calculations—was presented in Ref.[39]. Aside from our recent work on $2s2p\,^3P$ production from $1s2s\,^3S$ in He-like carbon and oxygen ions colliding with He[1], with comparisons to 3eAOCC and first Born results, little else has appeared since.

In the following, experimental and theoretical considerations in the production of the $2s2p\,^3P$ and $2s2p\,^1P$ states are discussed in sections 2 and 3, respectively. Section 4 provides a detailed critical analysis of theoretical and experimental cross-section results. Summary and conclusions are presented in section 5. The appendix includes tables of our 3eAOCC production cross sections, information on corrections due to SEC contaminants, fine-structure details related to the angular dependence of Auger emission at $\theta = 0^\circ$, tables of the determined metastable fractions, the thereupon computed theoretical normalized Auger yields compared to the measured Auger yields and tables of known measured and calculated Auger energies used for energy calibration and state identification.

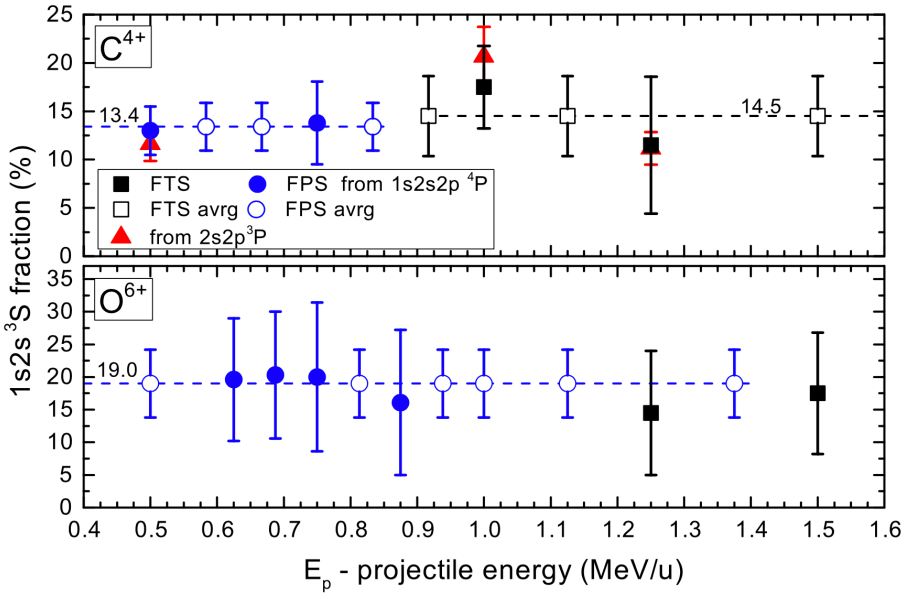

Figure 1. Experimentally determined $1s2s\,^3S$ ion beam fractions as a function of projectile energy E_p in MeV/u using the three-component model. (Top) C^{4+}, (Bottom) O^{6+} projectile ions. Where available, fractions were determined from either the $1s2s2p\,^4P$ (circles and squares) or the $2s2p\,^3P$ (red triangles) states, both of which are dominantly produced from the $1s2s\,^3S$ component. Good consistency is observed between the two determinations. Squares are from FTS, while circles from FPS)last stripper) measurements as given in Tables VII and VIII. Open symbols refer to values estimated by the mean value of similarly stripped ions (dashed lines), whose values appear in parentheses in the tables.

doi.org/10.32388/C8JRSC

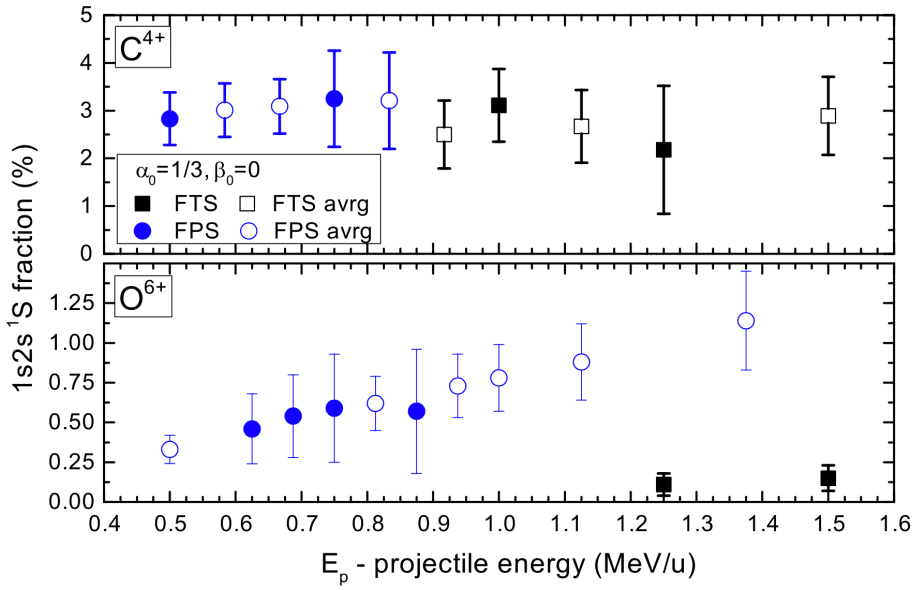

Figure 2. Same as Fig. 2, but for $1s2s\,{}^1S$ (with $\alpha_0 = 1/3$ and $\beta_0 = 0$ - see text). For oxygen, the much smaller values of $f[{}^1S]$ and their larger spread reflect the ~10 times shorter lifetime of the oxygen ${}^1S$ state compared to that of carbon. Since $f[{}^3S]$ is relatively constant over the same E_p range the rise of $f[{}^1S]$ with E_p reflects the decreasing time-of-flight Δt_0 in the negative exponential of Eq. 11. The smaller values for FTS stripping in oxygen are due to the longer Δt_0 required from the terminal stripper.

II. Experiment

The measurements reported here were taken during the same beam time reported in Ref.[1]. Experimental details of the setup and methodology was presented there so here only a very brief description is given. The experiment was conducted at the National Center for Scientific Research (NCSR) "Demokritos" 5.5 MV Tandem accelerator facility[40], utilizing our ZAPS setup centered around a hemispherical electron spectrograph with a pre-retardation lens and a doubly-differentially pumped gas cell, allowing for the detection of projectile Auger electrons with high efficiency and high energy resolution. Existing spectroscopic information about the KLL Auger lines also measured here used in the Auger energy calibration and the $2s2p$ Auger line identification is presented and compared to previous published results in tables found in appendix E.

A. Metastable fractions and their determination

The $1s2s\,{}^3S_1$ and $1s2s\,{}^1S_0$ states decay to the ground state predominantly by $M1$ and two-photon ($2E1$) transitions, respectively. They are therefore metastable[41] having relatively long lifetimes $\tau[{}^3S]$ and $\tau[{}^1S]$ (see Table I in Ref.[8]). Both these beam components can survive to the target[9] contributing, in general, to the production of the

doi.org/10.32388/C8JRSC

$2s2p\,^3P$ and $2s2p\,^1P$ states[23]. Using our "two-spectra" measuring technique[23][42], we are able to accurately determine, *in situ*, the $1s2s\,^3S$ beam fractional component $f[^3S]$, but not the $f[^1S]$ component. However, since the production of the $2s2p\,^1P$ depends sensitively on the $1s2s\,^1S$ component this component has to also be considered. Here, this component is estimated using our recently published three-component model[8].

According to the three-component model[8], the three fractions *at the target* are determined using our "two-spectra" measuring technique[23][42] by the following expressions:

$$f^{[1]}[^3S] = p\, f^{[2]}[^3S], \tag{5}$$

$$f^{[2]}[^3S] = \frac{(1-\beta^{[1]}) - d(1-\beta^{[2]})}{p(1+\alpha^{[1]}) - d(1+\alpha^{[2]})}, \tag{6}$$

$$f^{[i]}[^1S] = \alpha^{[i]} f^{[i]}[^3S] + \beta^{[i]}, \qquad \text{for } i = 1, 2, \tag{7}$$

$$f^{[i]}[1s^2] = 1 - f^{[i]}[^3S] - f^{[i]}[^1S] \qquad \text{for } i = 1, 2. \tag{8}$$

where p and d are the ratios of the ^4P and ^2D Auger yields measured in each of the two ($i = 1$ and $i = 2$) Auger spectra[8][23] given by

$$p \equiv \frac{dY_A^{[1]}[^4P]/d\Omega'}{dY_A^{[2]}[^4P]/d\Omega'}, \qquad d \equiv \frac{dY_A^{[1]}[^2D]/d\Omega'}{dY_A^{[2]}[^2D]/d\Omega'}, \tag{9}$$

where $dY_A^{[i]}[X]/d\Omega'$, represents the measured normalized Auger yield[23] for the Auger line X in measurement i. The parameters $\alpha^{[i]}$, $\beta^{[i]}$ are given by:

$$\alpha^{[i]} = \alpha_0^{[i]} \exp\left(\frac{\Delta t_0^{[i]}}{\tau[^3S]}\right) \exp\left(-\frac{\Delta t_0^{[i]}}{\tau[^1S]}\right), \tag{10}$$

$$\beta^{[i]} = \beta_0^{[i]} \exp\left(-\frac{\Delta t_0^{[i]}}{\tau[^1S]}\right), \tag{11}$$

where the metastable fractions at the point of their production (in the last stripper utilised - marked by the subscript 0) are assumed to be related by:

$$f_0^{[i]}[^1S] = \alpha_0^{[i]} f_0^{[i]}[^3S] + \beta_0^{[i]}. \tag{12}$$

Here, $\alpha_0^{[i]} = 1/3$ according to spin statistics, while $\beta_0^{[i]}$ is a parameter introduced in Ref.[8] to account for the production of ^1S in the stripper by singlet spin conserving excitation processes from the He-like ground state. Since there is no model yet to calculate β_0, we treat β_0 here as a free parameter with values in the range of 0-50%. The parameters $\alpha^{[i]}$ and $\beta^{[i]}$ then just propagate the ^1S fraction from the stripper, $f_0[^1S]$, to the target, $f[^1S]$, over the required time-of-flight, Δt_0, between the last stripper and the target[8].

In the two-spectra measurement technique both high and low ^3S fraction Auger spectra are used in the determination of $f[^3S]$[23]. However, the normalized yields presented here are obtained from the high ^3S fraction ($i = 1$) Auger spectrum which corresponds to larger $2s2p$ yields and therefore improved statistics. The determined high $f[^3S]$ fractions are shown in Fig. 1 for both carbon and oxygen computed according to Eqs. 5-6 and give the fractions at the target. Similarly, Fig. 2 gives the $f[^1S]$ fractions derived from the $f[^3S]$ fractions according to Eq. 7 for

$\beta_0 = 0$. For carbon, both $1s2s2p\,^4P$ and $2s2p\,^3P$ states were used in our technique since both states are predominantly produced from the $1s2s\,^3S$ component (a necessary requirement of the method). The good agreement underscores the consistency of the method. For some energies, where only one spectrum was measured (usually the high $f[^3S]$ measurement), the metastable fraction was estimated and marked in the tables with parentheses and with open symbols in Fig. 1. The fractions are also listed in Tables VII and VIII with stripping methods marked as gas terminal stripping (GTS), foil terminal stripping (FTS), gas post-stripping (GPS), foil post-stripping (FPS) and their combinations. These stripping methods are explained in more detail in Refs.[8][9]. Overall the ^3S metastable fraction over the energy range of the measurements remained rather constant around 13-14% for carbon and 19-20% for oxygen with the stripping methods used as seen in Fig. 1. The same is also seen in Fig. 2 (top) for the carbon ^1S fractions with a value of about 3%. However, this is not so for oxygen which due to its much shorter ^1S lifetime is much more sensitive to the stripper distance from the target and the speed of the ion beam[8] as seen in Fig. 2 (bottom).

B. Zero-degree normalized Auger electron yields

Normalized single differential Auger electron yields (for short normalized yields) at the observation angle θ, $dY_A(\theta)/d\Omega'$ are obtained from normalized double differential electron yields $d^2Y_A/d\varepsilon' d\Omega'$ (after transformation to the rest frame of the projectile indicated by primed quantities) by extracting the area under the Auger line of interest, typically using peak fitting software or SIMION[43] Monte Carlo simulations[24] for improved accuracy. In Ref.[19], we have described in detail how these normalized Auger yields were obtained in the case of the $1s2l2l'$ states produced by capture to the same mixed-state ion beams. In Figs. 3 and 4, the measured $\theta = 0^\circ$ normalized double differential electron yields are shown with the fitted areas of the $2s2p\ ^3P$ and ^1P Auger lines indicated, from which the normalized yields $dY_A^{\exp}/d\Omega'$ for the corresponding states were obtained. These are also listed in Tables VII and VIII and plotted as symbols with error bars in Figs. 10 and 11.

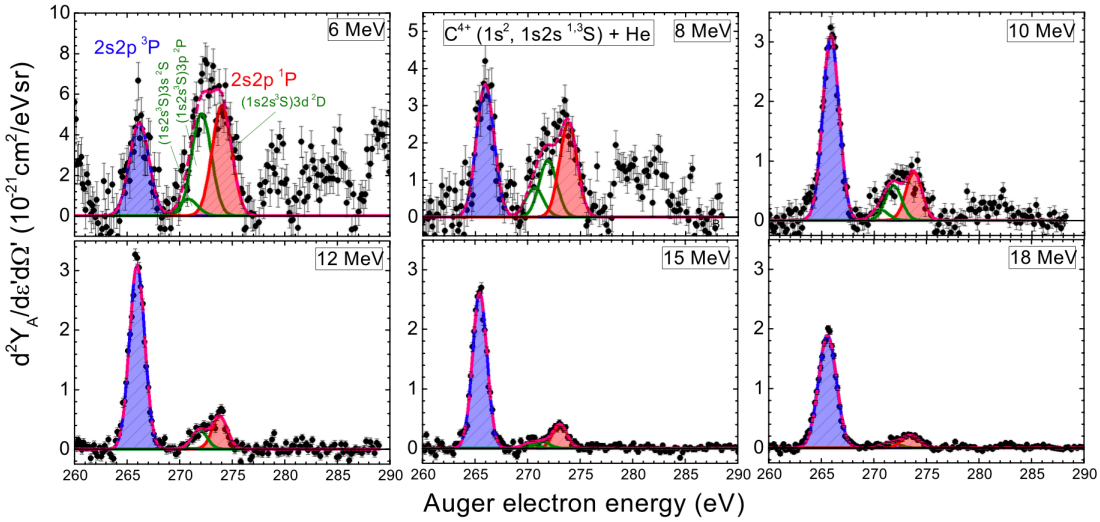

Figure 3. Normalized ZAPS spectra after background subtraction and transformation to the projectile rest frame as a function of electron energy at the selected projectile energies $E_p = 6, 8, 10, 12, 15, 18$ MeV in collisions of the C $^{4+}(1s^2,\ 1s2s\ ^{3,1}S)$ mixed-state ion beam with helium gas target. Identified in the shaded areas are both the $2s2p\ ^3P$ (blue) and $2s2p\ ^1P$ (pink) Auger lines. The stripping method and the extracted SDCS are listed in Table VII. The Gaussian fits in green correspond to the three near-lying Auger lines identified as the $(1s2s\ ^3S)3l\ ^2L$ with $l = 0, 1, 2$ and $L = l$ due to $3l$ capture to the $1s2s\ ^3S$ component (see Table IX). Particularly the $(1s2s\ ^3S)3d\ ^2D$ line lies within the pink shaded area and cannot be resolved from the $2s2p\ ^1P$. However, $3l$ capture is seen to drop rapidly with E_p, allowing for the ^1P line to be clearly identified at $E_p = 15$ MeV and above.

doi.org/10.32388/C8JRSC

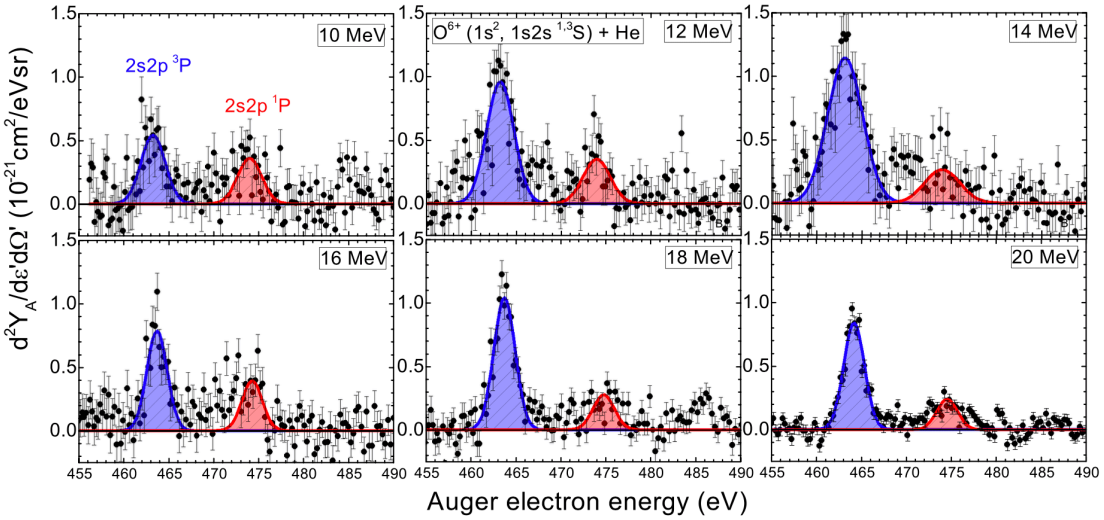

Figure 4. Same as Fig. 3, but for the $O^{6+}(1s^2,\ 1s2s\ ^{3,1}S)$ mixed-state ion beam at the selected projectile energies $E_p = 10, 12, 14, 16, 18, 20$ MeV. The stripping method and the extracted SDCS are listed in Table VIII. For oxygen there are no other troublesome Auger lines in between the two excitation lines as in the case of carbon.

C. Line identification

The $2s2p\ ^3P$ and ^1P Auger lines were identified in the normalized spectra shown in Figs. 3 and 4. At the lowest collision energies, for carbon, the ^1P line lies in between other partially overlapping $(1s2s\ ^3S)3l$ lines due to electron capture and can be difficult to identify. At the highest projectile energies, the two lines are the only ones left as capture has become negligible. To help in the unambiguous identification, we have provided in Table IX and Table X some indicative experimental and theoretical Auger energies of the various lines in the spectra. As seen from these tables the energies of the carbon $2s2p\ ^3P$ and ^1P Auger lines seem never to have been measured, while for the oxygen lines there seem to be only two such measurements one from collisions[44] and the other from dielectronic recombination[45]. Our own measured values are given in the first column of these tables. The well-known $1s2l2l'$ Auger lines[46] used to calibrate our spectra are also tabulated. The NIST reference energy levels (see Table II) were used to determine the theoretical Auger energies where needed. The relevant energy levels diagrams for both carbon and oxygen are shown in Fig. 14.

III. Theory

In Ref.[1], we presented 3eAOCC calculations for the production of $2s2p\ ^3P$ states from the $1s2s\ ^3S$ component [Eq. (1)] for both carbon and oxygen He-like ion beams. Here, we present only 3eAOCC results for the production of $2s2p\ ^1P$ states from all three beam components [(Eqs. (1)-(3)]. In addition, we also present 3eAOCC results for the production of the $2s2p\ ^3P$ states, including the other two initial components [Eqs. (2) and (3)].

doi.org/10.32388/C8JRSC

A. 3eAOCC calculations

The 3eAOCC method has been described in detail previously in[3][47][48][49] and already used in our single electron capture[18][19][50] and transfer-excitation[20] investigations in C^{4+} -He (and H_2) MeV collisions.

The 3eAOCC uses a semiclassical close-coupling approach based on a time dependent expansion of the scattering states onto sets of asymptotic states, i.e. states of the two isolated target and projectile partners of the collision. As in Ref.[1], the two collision systems are described here using a *three*-active electrons representation which allows for the accurate description of C^{4+} and O^{6+} after excitation including spatial and spin components (but neglecting spin-orbit coupling), as well as the final state of the target. Details of the 3eAOCC calculation for the process of Eq. (1) were provided in[1]. Here, the calculations using the same basis sets are also used to obtain production cross sections for the $2s2p\,^1P$ state, as well as for the production of both $2s2p\,^3P$ and $2s2p\,^1P$ states from the other two components, not addressed in Ref.[1].

For each of the three initial states of the He-like ion beam an independent 3eAOCC calculation was performed which included the production of both $2s2p\,^3P$ and $2s2p\,^1P$ states. For the target, one of the He electrons is considered frozen so that the interactions between the He^+ target core and the three active electrons is described by a model potential (see Table III in [19]). For the static (state and basis sets construction) and dynamical (collision) stages of the calculations, all Coulombic interactions and bi-electronic couplings were taken into account within a full configuration interaction scheme.

In the previous works we used very large basis sets to describe simultaneously one-electron processes (transfer, excitation and, in a more limited way, ionization) and two-electron processes (mainly transfer-excitation and double excitation). The present results therefore stem from the same computations for C^{4+} projectile: the same sets of Gaussian-Type Orbitals (GTO) for the genuine representation of the helium and carbon states (see Table II in [19]) were used. For oxygen projectile, we have an equivalent representation of the O^{6+} and O^{5+} states, with a set of 22 GTOs, 10 for ℓ=0 and 3×4 ℓ =1 symmetries, see Table I. With these GTO sets, the helium ground state is bound by 0.901 a.u. (to be compared to the NIST value of 0.9035698802 a.u.[51]) and the energies of the states for the C^{4+} and O^{6+} ions under consideration in the present work are shown in Table II. They are compared to reference values, with agreement better than $\sim$0.9% for carbon and $\sim$0.5% for oxygen.

ℓ		α	ℓ	α
0		3.00[-1]	0	1.30[2]
0		7.50[-1]	0	3.06[2]
0		1.77	0	1.73[3]
0		4.18	1	7.22[-1]
0		9.86	1	2.08
0		2.33[1]	1	6.80
0		5.49[1]	1	2.67[1]

Table I. Orbital angular momentum quantum numbers ℓ and exponents α of the GTOs $\mathcal{G}(r) = Nr^{\ell}\exp(-\alpha r^2)$ for oxygen ions. The notation 3.00[-1] stands for 3.00×10^{-1}. Note that the number of GTOs is 22 considering the multiplicity of 3 for each of the ℓ = 1 orbitals.

	C^{4+}		O^{6+}	
state	**present**	**NIST[a]**	**present**	**NIST[a]**
$1s^2\ ^1S$	-32.219	-32.409	-59.130	-59.193
$1s2s\ ^3S$	-21.314	-21.430[b]	-38.533	-38.578
$1s2s\ ^1S$	-21.114	-21.223	-38.246	-38.287
$2s2p\ ^3P$	-8.196	-8.234[b]	-14.949	-14.971
$2s2p\ ^1P$	-7.868	-7.939[c]	-14.498	-14.565

Table II. Energies (in a.u.) of states under direct consideration for C^{4+} and O^{6+} ions. The present values are compared with the ones listed in NIST[51] unless otherwise indicated.

[a] NIST - https://www.nist.gov/pml/atomic-spectra-database

[b] Mu ller *et al.* 2018[52].

[c] van der Hart and Hansen 1993[53].

For C^{4+} +He collisions, to solve the time-dependent Schrödinger equation, the time-dependent expansion of the scattering state spans the same Hilbert space as in[18], i.e. with a total 1794 3-electron bound, autoionizing and continuum states (799 of type C^{4+} × He and 995 of type C^{3+}) for doublet spin symmetry (respectively 802, 380 and 422 for quartet). For O^{6+} +He collisions, the basis set includes 1357 three-electron states, with 694 of O^{6+} × He and O^{5+} types, for doublet spin symmetry (respectively 598, 322 and 276 for quartet).

The cross sections stemming from the close-coupling computations and shown in the following are inclusive cross sections, i.e. cross sections for excitation to C^{4+} (2s2p) and O^{6+} (2s2p), whatever the final state of the helium target. This is mandatory since (i) the target is not analyzed experimentally after collision and (ii) our calculations prove that He excitation and ionization are very important channels, especially for initial metastable (1s2s $^{1,3}S$) helium-like ions.

Since the He-like Z^{q+} ions are in a mixture of the $1s^2$ ground state and the two long-lived $1s2s\,^3S$ and $1s2s\,^1S$ states, three independent calculations had to be performed one for each initial state as in the processes of Eqs. (1)-(3). Here, He(All) signifies that all final states of the He target were considered in the calculation, including the He$(1s)$, He(nl), and even ionization, i.e. He^+.

For the production of the $2s2p\,^{1,3}P$ states, the cross sections for the $M_L = 0$ component, $\sigma_j(M_L = 0)$, as well as the total (sum over M_L), $\sigma_j^{\rm tot}$, are listed in Tables III and IV as noted, for carbon and oxygen ion beams, respectively, where j signifies one of the three initial ion states, i.e. $1s^2$, ^3S and ^1S. In Figs. 5 and 6, the E_p energy dependence of the cross sections is shown.

B. Auger angular distributions and single differential cross sections

In an ion-atom collision the produced doubly-excited SLJ projectile state may Auger decay to a final $S_f L_f J_f$ state

$$(SLJ) \to (S_f L_f J_f) + e_A^-(\theta_e', \varepsilon_A;\, s = 1/2, \ell, j) \tag{13}$$

emitting an Auger electron e_A^- at angle θ_e' (the prime refers to the projectile rest frame) with respect to the initial beam direction with energy ε_A and ℓ orbital- and j total-angular momenta. The Auger SDCS are then angular distributions expressed as a sum over *even* (due to parity conservation) Legendre polynomials $P_k(\cos\theta_e')$ given by (see[19] and references therein):

$$\frac{d\sigma_A^j}{d\Omega'}(\theta_e') = \bar{\xi}\,\frac{\sigma_j^{\rm tot}}{4\pi}\left[1 + \sum_{k=2,4\ldots} a_k^j\, P_k(\cos\theta_e')\right], \tag{14}$$

where the index $j = 1s^2, ^3S, ^1S$, refers to the three different initial components of the ion beam and σ_j the production cross sections from each of these components to the $2s2p\,^{3,1}P$ states. The coefficients a_k^j can be theoretically computed in various approximations, $\sigma_j^{\rm tot}$ is the total state production cross section, while $\bar{\xi}$ is the mean Auger yield given in Tables VII-VIII for the two states.

For unresolved LSJ multiplets one has to sum over the various J levels in various formulations depending on whether the fine structure is in principle resolvable or not. Furthermore, the Auger electron might have more than one allowed ℓ or j angular momenta (see Eq. 13), in which case, further complications arise since the different partial (l,j)-waves can interfere. Examples of calculations in the LSJ intermediate coupling approximation are given in Refs.[54][55][56] and for LS coupling in Refs.[57][58].

In particular, for the P states ($L=1$) of interest here and for $k=2$ in Eq. (14), the coefficient a_2 is given by:

$$a_2^j = A_2^j D_2, \tag{15}$$

with the anisotropy coefficient A_2^j given by (see Table I of Ref. [58]):

$$A_2^j = 2\,\frac{\sigma_j[M_L=0]-\sigma_j(M_L=1)}{\sigma_j^{\rm tot}} \quad (j=1s^2,{}^3S,{}^1S) \tag{16}$$

$$\sigma_j^{\rm tot} = \sigma_j(M_L=0)+2\sigma_j(M_L=1), \tag{17}$$

and the dealignment factor D_2 (which accounts for the average loss of orbital alignment into spin alignment) is given by Eq. (C1). The partial production cross sections $\sigma_j(M_L)$ depend on the magnetic quantum number M_L and are computed in the 3eAOCC approach for each of the three initial beam components. They are listed for the production of the $2s2p\,{}^3P$ and ${}^1P$ states in Tables III and IV for collisions of carbon and oxygen ions with He target as already discussed in the Theory section. The anisotropy parameter is seen to take values from $A_2=2$, when $\sigma(M_L=1)=0$ to $A_2=-1$ when $\sigma(M_L=0)=0$ and thus is an indicator for alignment. And of course, when all partial cross sections are equal, then $A_2=0$ and we have isotropy. The anisotropy parameter is plotted in Fig. 5 for the two collision systems and states.

Evaluating Eq. (14) at the laboratory observation angle $\theta=0^\circ$ (for which $\theta_e'=0^\circ$ or 180° - see Eq. (27) in Ref.[19]), we then obtain for the Auger SDCS:

$$\frac{d\sigma_A^j}{d\Omega'}(0^\circ) = \bar{\xi}\,\frac{(1+2D_2)\sigma_j(M_L=0)+2(1-D_2)\sigma_j(M_L=1)}{4\,\pi}. \tag{18}$$

For no dealignment (completely overlapping resonances, i.e. $\varepsilon_{J,J'}=0$ in Eq. (C2) appendix C), $D_2=1$[58], and we get the well-known LS-coupling result:

$$\frac{d\sigma_A^j}{d\Omega'}(0^\circ) = \bar{\xi}\,\frac{3\,\sigma_j(M_L=0)}{4\,\pi}, \qquad (D_2=1) \tag{19}$$

while if all partial cross sections are equal, i.e. $\sigma_j\equiv\sigma_j(M_L=0)=\sigma_j(M_L=1)\,(=\sigma_j[M_L=-1])$, then $A_2^j=0$ [see Eq. (16)] and we have the case of isotropy as expected (independent of dealignment):

$$\frac{d\sigma_A^j}{d\Omega'}(0^\circ) = \bar{\xi}\,\frac{\sigma_j^{\rm tot}}{4\,\pi}, \qquad (\text{isotropic}) \tag{20}$$

which is seen to also correspond to the case of $D_2=0$. We note that for maximum dealignment, i.e. cases of extreme spin-orbit coupling encountered in much heavier projectiles, i.e. $\varepsilon_{J,J'}>>1$ (non-overlapping resonances), Eq. (C1) then gives $D_2=5/18=0.2778$ (see Eq. (23) of Ref.[58]). The relative overlap between the three resonances and its

effect on the value of D_2 is shown schematically in Fig.13 in appendix C. Its effect on the normalized yield compared to that for $D_2 = 1$ or isotropy is rather small.

C. Normalized Auger yields

Comparisons to the measured (normalized) $\theta = 0^\circ$ Auger yield, $dY_A^{\rm exp}(\theta = 0^\circ)/d\Omega'$ require the computation of the corresponding *total* theoretical normalized yields. These are calculated as the sum of the *partial* normalized yields from each one of the three j initial states:

$$\frac{dY_A^{\rm tot}}{d\Omega'}(\theta = 0^\circ) = \sum_j \frac{dY_A^j}{d\Omega'}(\theta = 0^\circ) \tag{21}$$

with $dY_A^j/d\Omega'$ are given by $\frac{dY_A^j}{d\Omega'}$:

$$\frac{dY_A^j}{d\Omega'}(\theta = 0^\circ) = f[j]\,\frac{d\sigma_A^j}{d\Omega'}(\theta = 0^\circ) \quad (j = 1s^2, {}^3S, {}^1S) \tag{22}$$

where $f[j]$ are the three fractional components of the mixed-state ion beam and $d\sigma_j^A(\theta = 0^\circ)/d\Omega'$ are the computed SDCSs according to Eqs. 18-20 discussed above and dependent on the 3eAOCC partial cross sections via the alignment parameter A_2 given by Eq. (16). The computed values of $dY_A^{\rm tot}/d\Omega'$ are listed in Tables VII and VIII and shown in Fig. 10 and 11.

IV. Results and discussion

In this section we present our measurements and theoretical results in both figures and tables and discuss the observed features. In all subsections, except the last, we assume that the metastable fractions are related just by spin-statistics as assumed in the past, i.e. $f_0[{}^1S] = (1/3) f_0[{}^3S]$, or $\beta_0 = 0$. In the last section, IV B 5, we explore non-zero values for β_0.

A. $2s2p\,{}^3P$ and $2s2p\,{}^1P$ production

1. 3eAOCC production cross sections

In Tables III and IV (see Appendix A) the 3eAOCC cross sections for the production of the $2s2p\,{}^{3,1}P$ states from each of the three initial states are tabulated as a function of collision energy E_p. They are also shown in Figs. 5 and 6 and discussed and compared with experimental data in the following.

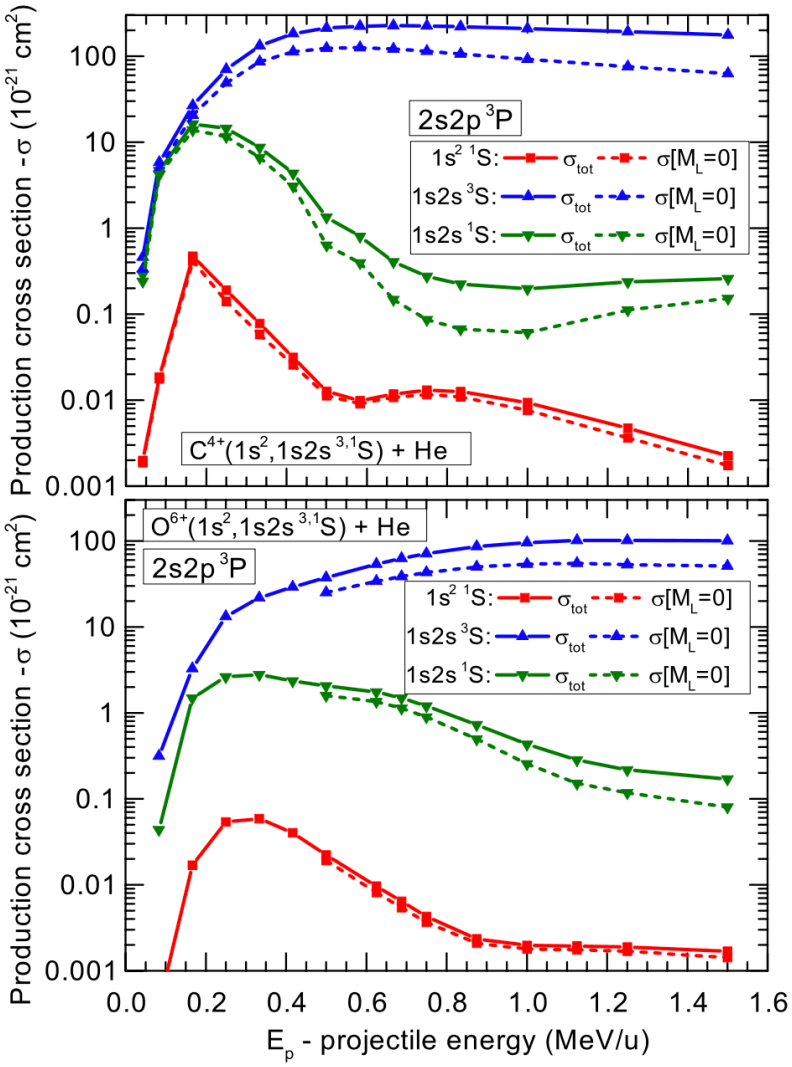

Figure 5. 3eAOCC $(2s2p\,^3P)$ production cross sections as a function of projectile energy E_p for C^{4+} (top) and O^{6+} (bottom) from each of the three different initial ion beam components in collisions with He: The $(1s2s\,^3S)$ state (blue lines with triangles), the $(1s2s\,^1S)$ state (green lines with inverted triangles) and the $(1s^2)$ ground state (red lines with squares). The full lines correspond to total cross sections (sum over all partial cross sections), while the dashed lines to just the $M_L = 0$ partial cross sections, $\sigma(M_L = 0)$ (where shown), as also listed in Table III and Table IV.

doi.org/10.32388/C8JRSC

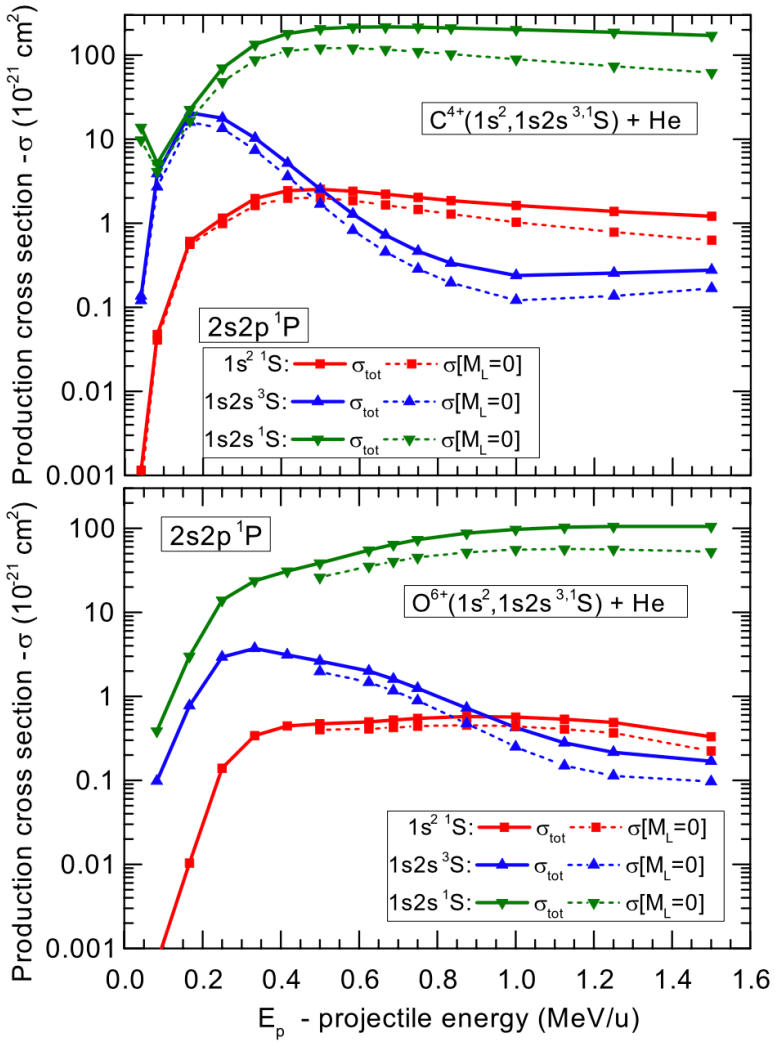

Figure 6. Same as Fig. 5, but for the production of the $2s2p\ ^1P$ state. Again, direct $1s \rightarrow 2p$ excitation, but from the $1s2s\ ^1S$ state (green lines with inverted triangles) is seen to be the dominant excitation mode, followed by $1s \rightarrow 2p$ excitation with exchange (blue lines with triangles) and double excitation (red lines with squares). Double excitation is seen to become larger than excitation with exchange as the collision energy E_p increases and the time allowed for spin exchange is correspondingly reduced.

2. Single excitation

As can be seen, single excitation without exchange [Eq. (1) for ^3P and Eq. (2) for ^1P] is by almost two orders of magnitude the dominant production mechanism (above $\sim$0.5 MeV/u for carbon and about $\sim$0.94 MeV/u for oxygen) exhibiting the well-known excitation E_p dependence: a low energy threshold followed by an increasing cross section

doi.org/10.32388/C8JRSC

eventually dropping off slowly with increasing energy E_p. For these triplet to triplet and singlet to singlet excitations their Q values are very similar (see Fig. 14) which might explain their very similar energy dependence. However, excitation with spin exchange [Eq. (1) for ^1P and Eq. (2) for ^3P], while having a similar low E_p behavior, falls off much more rapidly than direct excitation. Thus, it seems spin exchange is much more probable at the lowest collision energies, where more time is available for the spin exchange to occur.

3. Double-excitation

Overall, as seen in Figs. 5 and 6, the double-excitation process (red squares - excitation from the initial projectile ground state) is by far the weakest, followed by single excitation with exchange (green inverted triangles), while direct single excitation (blue triangles) is seen to be the strongest. These general features are seen to apply to both carbon and oxygen, even though for oxygen the low E_p energy region close to threshold is not covered. Interestingly though, for the $2s2p\,^1P$ and E_p energies larger than $\sim$6 MeV (0.5 MeV/u) for carbon and $\sim$15 MeV (0.94 MeV/u) for oxygen, double-excitation without spin exchange seems to become more efficient than single-excitation with exchange. And of course, double-excitation with spin exchange needed in the production of $2s2p\,^3P$ from the ground-state is seen to be the weakest process.

Finally, the $\sigma(M_L = 0)$ partial cross section is seen to follow very closely the total cross section in its energy dependence. More on the difference between the $M_L = 0$ and the $M_L = 1$ partial cross sections can also be gained from the anisotropy parameter A_2^j discussed next.

4. Anisotropy parameters A_2

The anisotropy coefficient A_2 gives important information about the alignment of the states due to excitation. From Eq. (16) it is clear that minimum alignment is attained when the $M_L = 0$ and $M_L = 1$ partial cross sections are equal in which case $A_2 = 0$ resulting also in the isotropic distribution of the Auger emission. Extreme alignment occurs when one of the two partial cross sections is zero. Then, A_2 is positive with $A_2^j = 2$, when $\sigma_j(M_L = 1) = 0$ or negative with $A_2^j = -1$, when $\sigma_j(M_L = 0) = 0$.

In Fig. 7 the anisotropy parameter A_2^j is plotted as a function of collision energy E_p for excitation from each of the three initial beam components $j = 1s^2\,^1S, 1s2s\,^3S, 1s2s\,^1S$ for both $2s2p\,^3P$ and $2s2p\,^1P$ for carbon and oxygen, respectively. All three initial state excitation processes seem to be preferentially populated in the $M_L = 0$ state with the process of double-excitation with spin exchange being the most strongly aligned, both for carbon, but particularly for oxygen. The exception seems to be the excitation of the $2s2p\,^3P$ state from the $1s2s\,^1S$ state of carbon for which A_2 drops strongly, even attaining negative values, in the energy range of 6-18 MeV. Interestingly, in the same rough energy range A_2 for $2s2p\,^3P$ excitation from the ground state seems to take on its most positive values approaching the maximum of 2. Oxygen seems to also demonstrate a similar energy dependence, but with much less variation.

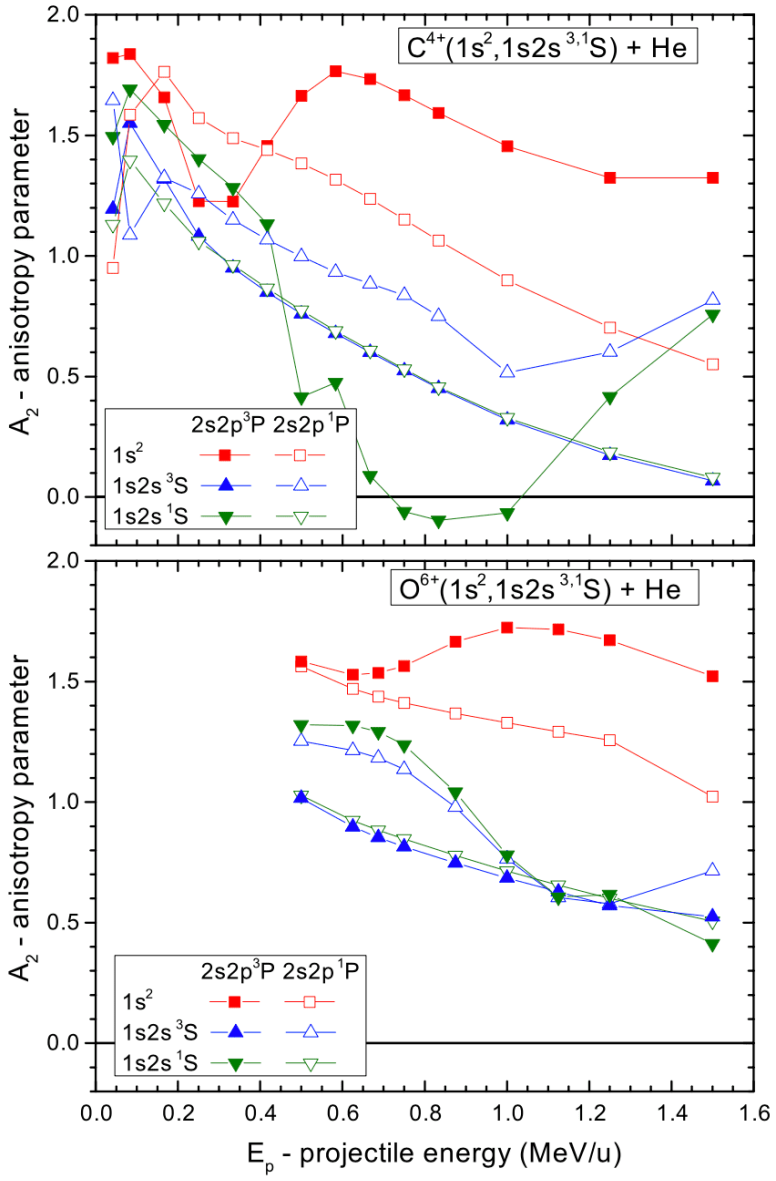

Figure 7. Anisotropy parameter A_2 [see Eq. (16)] for $2s2p\,^3P$ (filled symbols) and $2s2p\,^1P$ (open symbols) as a function of projectile energy E_p for each one of the three initial states in collisions of C^{4+} (top) and O^{6+} (bottom) with He. Direct excitation for both ^3P (blue triangles) and ^1P (green inverted triangles) is seen to show very similar behavior. For the oxygen energy points below 0.5 MeV/u, which are outside the range of the measurements, no partial cross sections were computed and therefore no A_2 values are shown.

doi.org/10.32388/C8JRSC

5. $2s2p$ excitation ratio - $\sigma(^3P)/\sigma(^1P)$

In Fig. 8 the computed cross section ratios for direct and exchange single excitation for carbon and oxygen are shown, respectively.

For the process of direct excitation [Eq. (1) for ^3P and Eq. (2) for ^1P], this ratio involves the production cross sections of ^3S to ^3P and of ^1S to ^1P. This ratio is found to be nearly 1 for carbon and slightly below 1 for oxygen, remaining almost constant across the full range of projectile energies, except at the lowest energy points for both ions. This near-identical behavior suggests a similar underlying excitation mechanism. The $M_L = 0$ ratios show a similar trend as well.

However, for the process of exchange excitation [Eq. (1) for ^1P and Eq. (2) for ^3P] the behavior is very different with this ratio dropping much below 1 above 0.5-0.6 MeV/u, while increasing back to near 1 with increasing collision energy, and also surpassing 1 at the very low collision energies. This might indicate a different excitation mechanism with the production of the $2s2p\,^1P$ via spin exchange being more probable than that for $2s2p\,^3P$. However, for oxygen this doesn't seem to be the case since both ratios for direct and exchange excitation are seen to have almost identical behavior as a function of E_p, except at the lowest collision energies.

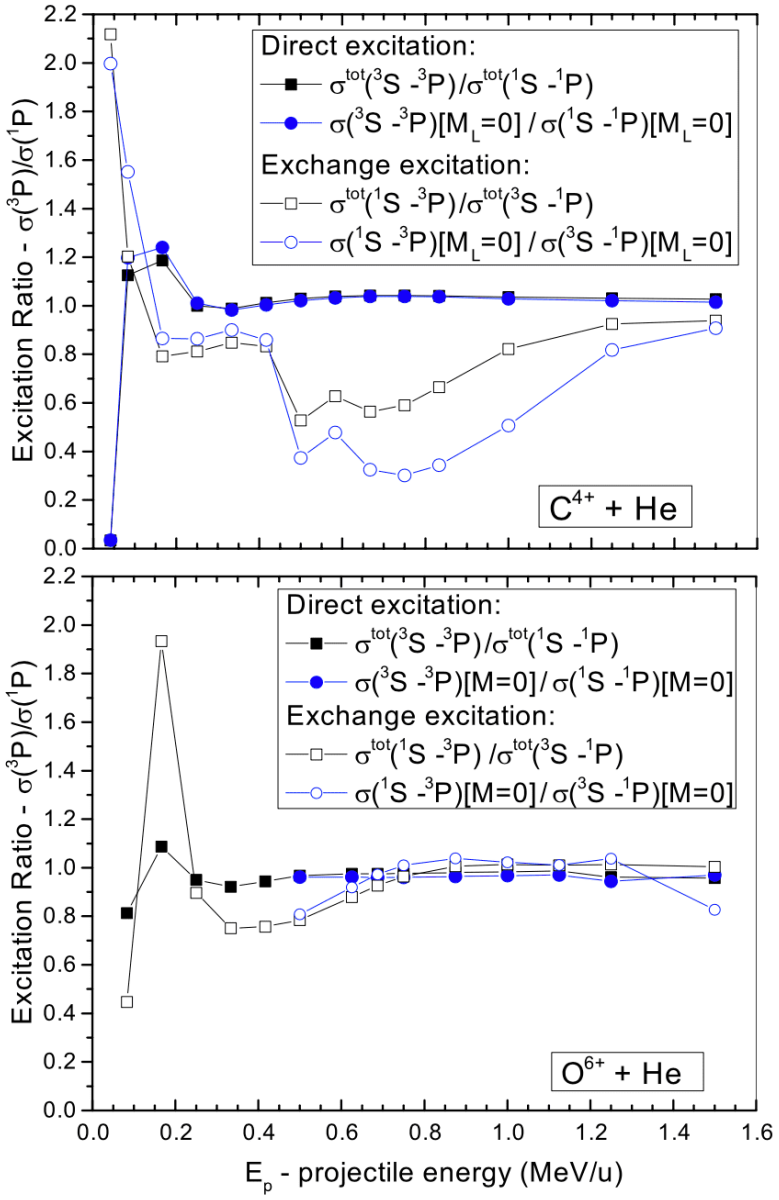

Figure 8. Ratio of $2s2p\,^3P$ to $2s2p\,^1P$ cross sections for C^{4+} (top) and O^{6+} (bottom). Direct excitation: Total cross sections (black squares), $M_L = 0$ partial cross sections (blue circles). Exchange excitation: Total cross sections (black open squares), $M_L = 0$ partial cross sections (blue open circles).

6. Impact parameter dependence

The reduced probabilities $bP(b)$ of carbon are shown in Fig. 9 for $2s2p\,^3P$ (left) and for $2s2p\,^1P$ (right) production from each of the three initial components of the ion beam. These calculations were performed out to a maximum impact parameter of 5.0 a.u., but already after about 1.4 a.u., $bP(b)$ is seen to be practically zero. In the figures, we

doi.org/10.32388/C8JRSC

only show the range from $b = 0 - 1.4$ a.u. No indication of a large impact parameter b component is seen that could signal the onset of a two-center electron-electron (TCee) interaction as was reported in the case of resonance transfer-excitation (RTE) in C^{4+} collisions with He using a similar 3eAOCC calculation[20]. Such a TCee excitation might be expected in the case of excitation with spin exchange already observed in the case of the production of the $1s2s2p\,^4P$ state in O^{5+} and F^{6+} Li-like $(1s^22s)$ ions in collision with He and H_2[59]. Here, such an excitation with spin exchange should also be active in the production of the $2s2p\,^1P$ and $2s2p\,^3P$ from the $1s2s\,^3S$ and $1s2s\,^1S$ initial beam components, respectively. However, no such signature is observed in the impact parameter dependence.

This seems to be consistent with the lack of any clear TCee excitation collisional energy thresholds observed neither in the impact parameter dependence nor in the corresponding cross sections as observed in Ref.[60].

In Fig. 9, we also observe the important drop (at least one order of magnitude) of the reduced probabilities for the spin exchange excitation processes, compared to spin conserved (direct) excitation, the consequence of which is the related weaker cross sections seen in Figs. 5 and 6. Moreover, the impact parameter extent of the probability for these processes is seen to be somewhat reduced indicating spin exchange processes require more violent collisions to happen. This fact is even more pronounced for low velocity collisions involving the projectile $1s^2\,^1S$ ground state, also due to the smaller spatial extent of this state compared to the metastable ones. Similar observations can also be made for O^{6+} collisions.

doi.org/10.32388/C8JRSC

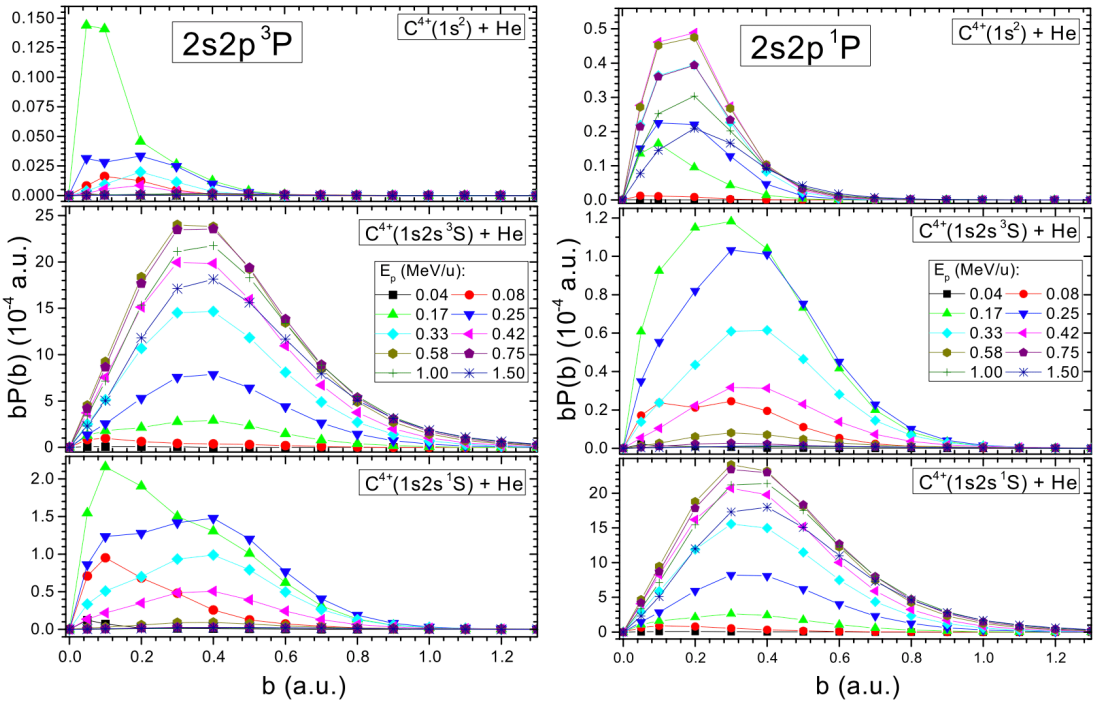

Figure 9. Reduced probabilities $bP(b)$ plotted as a function of impact parameter b for selected characteristic projectile energies E_p. (Left) $2s2p\,^3P$ production, (Right) $2s2p\,^1P$ production. (Top) From the $C^{4+}(1s^2)$ ground state, (Middle) From the $C^{4+}(1s2s\,^3S)$, and (Bottom) From the $C^{4+}(1s2s\,^1S)$ metastable states. Calculations are for the total probabilities (sum over all M_L and all final target states included in the calculation).

doi.org/10.32388/C8JRSC

B. Normalized Auger yields

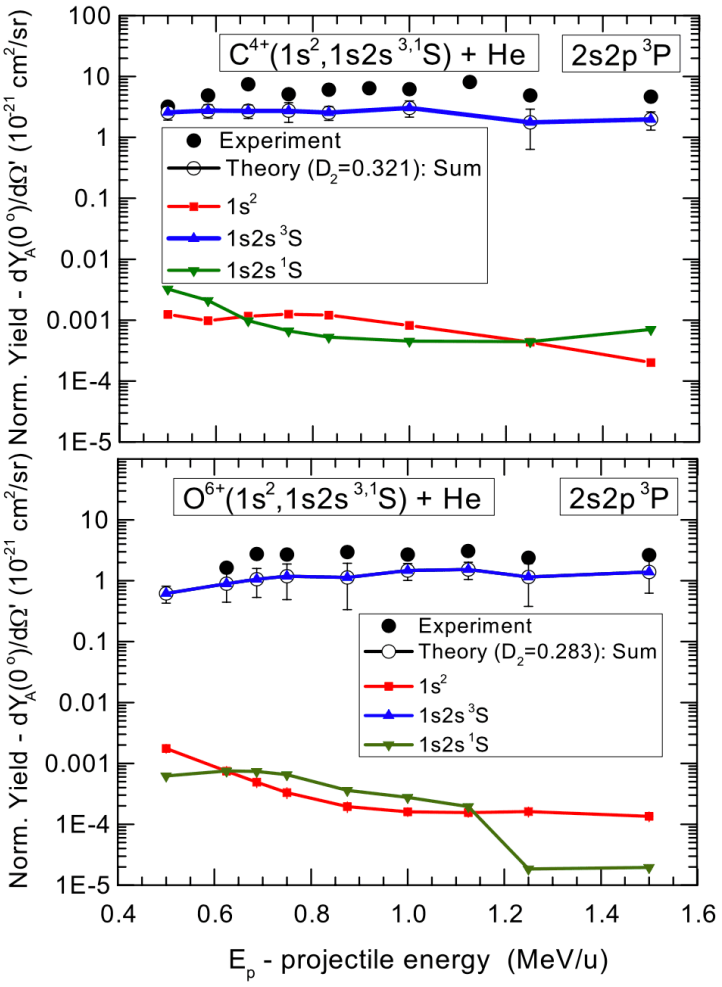

Figure 10. Zero-degree Auger normalized yields for the production of the $2s2p\,^3P$ from each of the three ion beam components with $D_2 = 0.321$ for C^{4+} (top) and $D_2 = 0.283$ for O^{6+} (bottom). Black circles: Measured normalized yields. Contributions from the $1s2s\,^3S$ beam component (blue line with triangles) dominate as the sum of the three contributions (black line with circles) hides behind the contribution of the $1s2s\,^3S$ beam component. The uncertainty in the theoretical results includes the uncertainties in the beam component fractions (see text) and the 3eAOCC cross sections (∼15%) added in quadrature. Error bars shown on the experimental values include only the statistical uncertainty.

doi.org/10.32388/C8JRSC

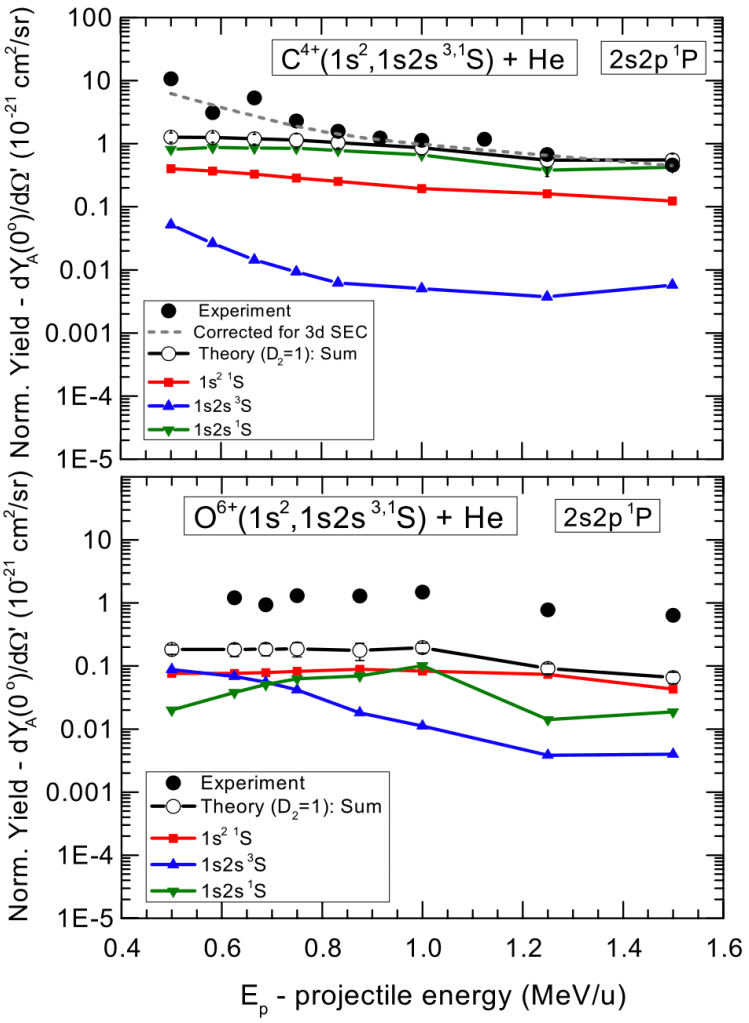

Figure 11. Same as Fig. 10, but for the $2s2p\,^1P$ with $D_2 = 1$. In the case of carbon (top) contributions from the $1s2s\,^1S$ are seen to be the most important, but the ground state contributions cannot be neglected as they are only about a factor 3-5 smaller. Grey circles (top): Estimated contribution of the blended $(1s2s\,^3S)3d\,^2D$ Auger line due to $3d$ SEC to the $1s2s\,^3S$ component has been subtracted (see Appendix B for more details).

1. Comparison to experiment for $\beta_0 = 0$

In Figs. 10 and 11 the computed normalized Auger yields from each initial state [Eq. 22] and their sum $dY_A^{\rm tot}(0^\circ)/d\Omega'$ [Eq. (21)] for $\beta_0 = 0$ are compared to the measured normalized Auger yields $dY_A^{\rm exp}(0^\circ)/d\Omega'$ for the $2s2p\,^3P$ and $2s2p\,^1P$ states. In the case of the carbon $2s2p\,^1P$ production [Fig. 11 (top)], the estimated contribution of the $(1s2s\,^3S)3d\,^2D$ Auger line [produced by single electron capture (SEC) - which could not be resolved - see appendix B] was subtracted, slightly improving the overall agreement between theory and experiment at the lowest

doi.org/10.32388/C8JRSC

energies. Numerical results are also listed in Tables VII and VIII together with the determined fractional beam components.

The calculated total normalized Auger yields $dY_A^{\rm tot}(0^\circ)/d\Omega'$ for $C^{4+}(2s2p\,^3P)$ are seen in Fig. 10 (top) to be roughly within a factor of 2 of the measured normalized Auger yields and in good overall agreement as to their E_p-dependence with what was already reported in Ref.[1], where the approximation Eq. (3) was used there instead of the full contribution Eq. (21). Similarly, for $C^{4+}(2s2p\,^1P)$, excellent agreement is found for $E_p > 0.8$ MeV/u, but an increasing discrepancy is observed with decreasing E_p, even after subtraction of the contamination due to the $(1s2s\,^3S)3d\,^2D$ state.

The normalized Auger yield calculations for carbon excitation show that the production of the ^3P is dominantly due to *direct* single excitation from the $1s2s\,^3S$ beam component [Eq. (1)] by almost three orders of magnitude justifying the use of the approximate Eq. (3) in Ref.[1]. Similarly, the production of the ^1P state by direct single excitation [Eq. (2)] is also seen to dominate, even though the beam fraction $f[^1S]$ is smaller (see Table VII). However, now the ground state contributions are also seen to be important as they are roughly only about a factor of 2 smaller, mainly due to the about 20 times larger ground state fraction.

A similar picture is also seen to hold for the oxygen $2s2p\,^3P$ state with agreement being slightly better than for carbon as seen in Fig. 10 (bottom). However, for the oxygen $2s2p\,^1P$ state, the agreement with experiment is seen quite a bit worse, with experiment being larger by factors of more than 2-5, as seen in Fig. 11 (bottom). In the case of oxygen, the $1s2s\,^1S$ component is seen to be much weaker (less ions survive to the target due to the much shorter lifetime), at only about 0.10-0.79% (see Table VIII). Thus, as also seen for carbon, production from the ground state is now relatively enhanced because of the much larger ground state fraction. Finally, also similarly to carbon, contributions from excitation with exchange (i.e. from the ^3S) is seen to be more than an order of magnitude smaller than from the ground state, particularly at the highest projectile energies.

It is notable that the oxygen $f[^1S]$ fractions for $\beta_0 = 0$ remains very small, primarily due to its significantly shorter lifetime. Consequently, even a substantial increase in its value — by a factor of about 10 — would have minimal impact on the other two components of the He-like ion beam, yet would significantly help in narrowing the observed discrepancy between theory and experiment for $2s2p\,^1P$ production. This could occur for β_0 values larger than 0, as shown in Ref.[8].

Our three-component model with $\beta_0 = 0$ assumes that ^1S production is tied to ^3S in a 1:3 ratio, as dictated by statistical considerations[12]. This approach has been applied previously in studies of low-energy capture to He $^+(1s)$ forming metastable $\mathrm{He}(1s2l^{\,3,1}l)$ states[61][62], capture into He-like $1s2s\,^3S$ ions in carbon yielding $1s2l2l'$ states[18][19], and dielectronic recombination (DR) measurements of He-like ions with electron coolers[12]. The assumption has also been used in $1s$ loss studies for Be-like carbon and oxygen resulting in $1s2l2l'$ states[63] and in Li-like low-Z_p ions for $1s2s^{\,3,1}S$ states[15]. However, while plausible, this assumption may warrant further scrutiny

as recently spin statistics has been found not always to apply[18][64][65], highlighting the need for additional investigation. In section IV B 5 we explore three-model results with $\beta_0 > 0$.

2. Differences in the Auger angular distributions

The comparison with experiment are shown in the previous normalized yield figures only for the computed values of the anisotropy parameter corrected by the dealignment parameter D_2. In the case of the ^1P there is no such correction since this state has no fine structure splitting and therefore $D_2 = 1$. Typically, most calculations make rather rough estimates of the angular distributions either assuming isotropy and/or ignoring alignment. In Fig. 13 the normalized yields for the three different cases are compared. The largest differences are seen to be of the order of 40% between isotropic and $D_2 = 0.321$ and slightly bigger in the case of oxygen. Overall, using the correct D_2 value seems to improve the discrepancy between theory and experiment.

3. Validity of a one-electron model for the He target for projectile excitation

As already mentioned our production cross sections for excitation calculated in the 3eAOCC approach assumed a one-electron model for the He target. Thus, the question arises whether it would be more correct to assume further an independent electron approximation (IEA) for the He target and multiply our results by 2 (see also discussion in Ref.[1]), as was done in the case of SEC[19] and transfer-excitation[20]. This correction seemed to be justified within an OBK simplified model and therefore was adopted in that work. In the case of excitation, the IEA is rather confusing. The terms appearing in the three-electron (3e) OBK formulation would also be found in a four-electron (4e) formulation and indeed also multiplied by 2 (when shared). However, there are many additional terms appearing in the 4e OBK which are clearly not negligible. Therefore, we feel it is not legitimate to apply a multiplication factor of 2 in this case. Here, we have tried to include all relevant factors (Auger angular distributions with corrections for fine structure effects and alignment, partial cross sections with dependence on M_L, fractional composition of the He-like ion beam) and in our 3eAOCC treatment all couplings to other non-negligible states, as well as contributions from all three initial states.

In addition, it should be reminded that in our 3eAOCC treatment both the interaction with the target nucleus, as well as with the target electron are treated on the same footing and thus included coherently for the first time. In the past, the factor of 2 has been applied to theoretical calculations of two-center electron-electron interactions (also called electron-electron excitation (eeE)[60][66][67] or electron impact excitation (EIE)[68]) performed within the impulse approximation. These eeE results were then added incoherently to the excitation due to the interaction with the target nucleus (referred to as electron-nucleus excitation (enE)[60] or proton impact excitation (PIE)[68]). Clearly, a 4eAOCC treatment would be more appropriate, but for the time being is just too difficult and time consuming making it impractical for the present.

4. *Cascade contributions*

The possibility of cascade contributions was already discussed[1] and found negligible in the case of $2s2p\,^3P$ excitation, basically due to the low radiative branching ratios for cascade feeding by dipole transitions from higher lying $2snl\,^3L$ states which can also be excited. Similarly, higher lying $2snl\,^1L$ states can also be excited and can similarly be expected to have small radiative branching ratios. Thus, $2s2p\,^1P$ excitation can also be expected to have minimal contributions from cascades. Of course, radiative branching ratios increase roughly as Z_p^4 so excitation of higher Z_p projectiles would be increasingly prone to such radiative cascade feeding.

doi.org/10.32388/C8JRSC

5. Comparison to experiment for $\beta_0 > 0$

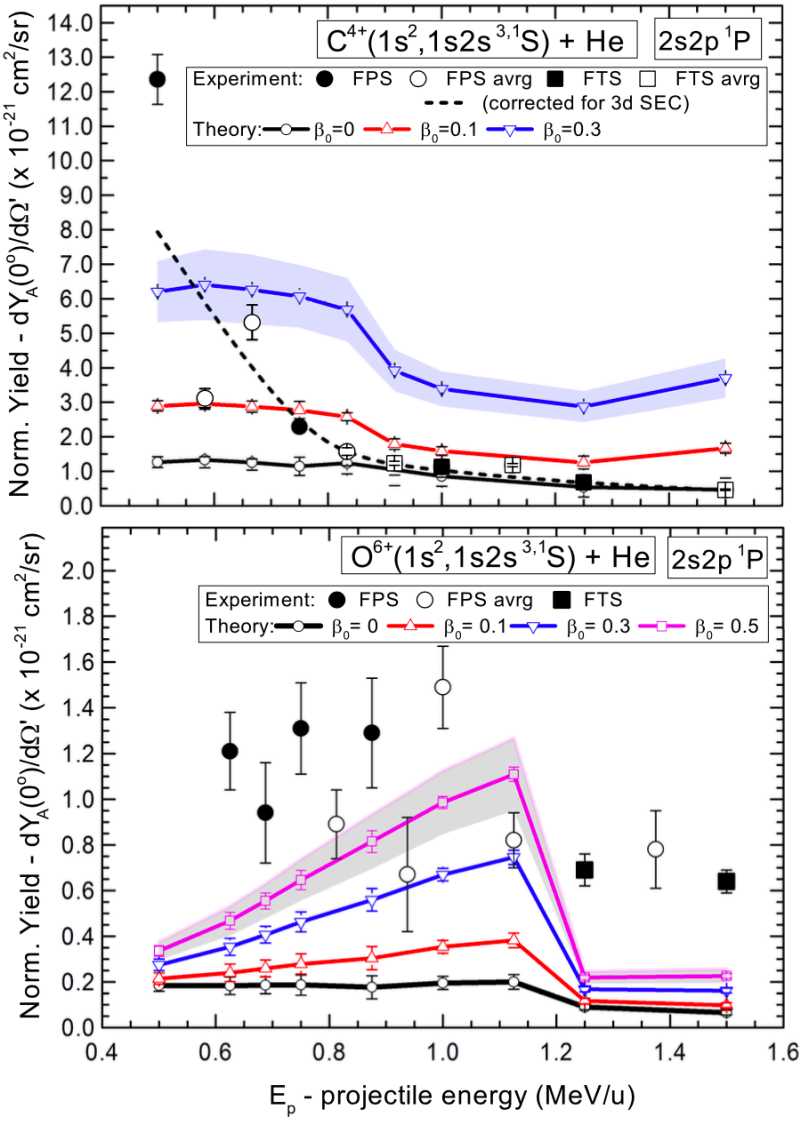

Figure 12. Comparison of experimental (same as in Fig. 11, but with last stripper indicated) and theoretical ($D_2 = 1$ - sum of all three contributions) normalized Auger yields for the production of the $2s2p\ ^1P$ state in C^{4+} (top) and O^{6+} (bottom) in collisions with helium as a function of projectile energy. For carbon the dashed line indicates the estimated experimental results after subtraction of $1s2s3d\ ^2D$ contributions. The theory has been weighted by the three-component model fractions according to Eq. 21 with $f[^1S]$ parameterized by β_0 (see Eqs. 7 and 12). The error bars on both experiment and theory are purely statistical. The shaded zones also include a maximum theoretical uncertainty of 15% in the 3eAOCC calculation of the production cross sections (indicated only for $\beta_0 = 0.3$ for C^{4+} and $\beta_0 = 0.5$ for O^{6+}). The $\beta_0 = 0$ results are the same as shown

doi.org/10.32388/C8JRSC

in Fig. 11. Increasing the value of β_0 is seen to close the gap between theory and experiment for oxygen, while it does not seem to help much in the case of carbon.

The large discrepancy between theory and experiment observed for $\beta_0 = 0$, particularly for the $2s2p\,^1P$ level, suggests the need for comparisons using larger values of $f[^1S]$, which can be controlled by non-zero values of β_0. In Ref.[8], we demonstrated that using $\beta_0 > 0$ values, while remaining consistent with previous studies, improves this agreement.

In Fig. 12, theoretical normalized Auger yields are calculated now also using β_0 values ranging from 0–30% for carbon and 0–50% for oxygen. As β_0 increases, $f[^1S]$ fractions grow significantly, while $f[^3S]$ and $f[1s^2]$ decrease only slightly, by just a few percent[8]. Therefore, Fig. 12 presents (on a linear scale) the effect of β_0 on the final summed yield, $dY_A^{\rm tot}/d\Omega'$.

As discussed in Ref.[8], no measurements of the $f[^1S]$ fraction currently exist, and all value estimates rely on statistical assumptions, such as Eq. 12 with $\alpha_0 = 1/3$ and $\beta_0 = 0$ (e.g., see[69]). Non-zero values of β_0, which imply a larger-than-expected ^1S fraction, were considered for the first time in Ref.[8].

V. Summary and Conclusions

We have presented theoretical and experimental results for the production of $2s2p\,^3P$ and $2s2p\,^1P$ states in 0.5-1.5 MeV/u collisions of He-like mixed-state ($1s^2$, $1s2s\,^3S$ and $1s2s\,^1S$) carbon and oxygen ion beams with He. A nonperturbative, three-electron treatment was used to calculate the cross sections for the production of these doubly excited states from each of the three possible initial ionic states. In parallel, the production of these states was also experimentally determined using high-resolution Auger projectile spectrography at $\theta = 0^\circ$ with respect to the beam direction. The $1s2s\,^3S$ metastable component was also determined experimentally, while the $1s2s\,^1S$ component was assumed to be statistically produced in the ratio of 3:1 according to the $1s2s\ ^3S$ to ^1S spin degeneracies and was included in a more complete three-component analysis. The effects of dealignment due to fine structure splitting were also included in the Auger angular distributions at the observation angle of $\theta = 0^\circ$. Thus, using this three-component fractional composition the $\theta = 0^\circ$ theoretical normalized yields were determined and compared to the measured mixed-stated normalized yields.

In all cases, the measured yields were higher than the theoretical predictions. For carbon, the yields exceeded theory by factors ranging from 1.7 to 4.2 for the $2s2p\,^3P$ state, and from 1.2 to 6.2 for the $2s2p\,^1P$ state. For oxygen, these factors ranged from 1.8 to 2.6 for the $2s2p\,^3P$ state, and from 3.6 to 7.6 for the $2s2p\,^1P$ state, with the disagreement being significantly larger for the $2s2p\,^1P$ state compared to the $2s2p\,^3P$.

An alternative interpretation of these disagreements could be due to a novel, unknown, mechanism not described in the present close-coupling calculations, involving eventually, both target electrons, while presently the activity of

only one is taken into account in our three-electron approach. However, it's hard to imagine how such a mechanism could account for the large up to factor of 10 disagreement. The larger discrepancy for the $2s2p\,^1P$ states may also result from an underestimation of the ^1S fraction in our three-component model with $\beta_0 = 0$. Increasing the values of β_0 increases the ^1S fraction showing improved agreement between theory and experiment, particularly for oxygen. This suggests that the ^1S fraction might be higher than anticipated in the $\beta_0 = 0$ models.

Overall, our 3eAOCC calculations are the most advanced of their kind to date and applied for the first time to describe excitation. Clearly, more systematic isoelectronic investigations are needed to shed further light on these new results and the observed disagreement with experiment. In addition, more work on better defining the amount of the $f[^1S]$ fraction in He-like ion beams either theoretically or experimentally would clearly also be very helpful.

Acknowledgments

We would like to thank the personnel of the "Demokritos" Tandem for their help with the measurements. We acknowledge partial support of this work by the project "CALIBRA/EYIE" (MIS 5002799) which is implemented under the Action "Reinforcement of the Research and Innovation Infrastructure", funded by the Operational Programme "Competitiveness, Entrepreneurship and Innovation" (NSRF 2014-2020) and co-financed by Greece and the European Union (European Regional Development Fund).

Appendix A. 3eAOCC excitation cross sections

		$C^{4+}(1s^2, 1s2s\ ^{3,1}S) + He \rightarrow C^{4+}(2s2p\ ^{3,1}P) + He(All)$					
V_p [a]	E_p	$C^{4+}(1s^2)$		$C^{4+}(1s2s\ ^3S)$ [b]		$C^{4+}(1s2s\ ^1S)$	
		$\sigma(M_L=0)$	σ^{tot}	$\sigma(M_L=0)$	σ^{tot}	$\sigma(M_L=0)$	σ^{tot}
(a.u.)	(MeV)	[$\times 10^{-21}$ cm^2]					
		$2s2p\ ^3P$:					
1.291	0.5	1.87[-3]	1.99[-3]	3.36[-1]	4.59[-1]	2.40[-1]	2.89[-1]
1.826	1	1.76[-2]	1.86[-2]	4.95	5.82	4.19	4.67
2.582	2	4.16[-1]	4.70[-1]	2.06[1]	2.67[1]	1.38[1]	1.63[1]
3.162	3	1.41[-1]	1.89[-1]	4.87[1]	7.02[1]	1.16[1]	1.45[1]
3.652	4	5.77[-2]	7.79[-2]	8.61[1]	1.32[2]	6.62	8.70
4.082	5	2.57[-2]	3.13[-2]	1.13[2]	1.83[2]	3.08	4.33
4.472	6	1.13[-2]	1.27[-2]	1.24[2]	2.11[2]	6.32[-1]	1.34
4.830	7	9.10[-3]	9.88[-3]	1.25[2]	2.24[2]	3.95[-1]	8.04[-1]
5.164	8	1.07[-2]	1.18[-2]	1.21[2]	2.27[2]	1.48[-1]	4.07[-1]
5.477	9	1.16[-2]	1.30[-2]	1.14[2]	2.24[2]	8.60[-2]	2.75[-1]
5.774	10	1.09[-2]	1.26[-2]	1.06[2]	2.20[2]	6.72[-2]	2.23[-1]
6.325	12	7.63[-3]	9.32[-3]	9.20[1]	2.09[2]	6.12[-2]	1.96[-1]
7.071	15	3.64[-3]	4.69[-3]	7.53[1]	1.92[2]	1.12[-1]	2.36[-1]
7.746	18	1.74[-3]	2.25[-3]	6.26[1]	1.76[2]	1.52[-1]	2.59[-1]
		$2s2p\ ^1P$:					
1.291	0.5	7.48[-4]	1.15[-3]	1.20[-1]	1.36[-1]	9.80	1.38[1]
1.826	1	4.08[-2]	4.73[-2]	2.70	3.88	4.13	5.17
2.582	2	5.61[-1]	6.09[-1]	1.60[1]	2.06[1]	1.66[1]	2.25[1]
3.162	3	9.88[-1]	1.15	1.34[1]	1.78[1]	4.82[1]	7.02[1]
3.652	4	1.63	1.96	7.36	1.03[1]	8.77[2]	1.34[2]
4.082	5	1.98	2.44	3.58	5.19	1.12[2]	1.80[2]
4.472	6	2.01	2.52	1.69	2.54	1.21[2]	2.05[2]

doi.org/10.32388/C8JRSC

		$C^{4+}(1s^2, 1s2s\,^{3,1}S) + He \rightarrow C^{4+}(2s2p\,^{3,1}P) + He(All)$					
V_p [a]	E_p	$C^{4+}(1s^2)$		$C^{4+}(1s2s\,^3S)$ [b]		$C^{4+}(1s2s\,^1S)$	
		$\sigma(M_L=0)$	σ^{tot}	$\sigma(M_L=0)$	σ^{tot}	$\sigma(M_L=0)$	σ^{tot}
(a.u.)	(MeV)	[$\times 10^{-21}$ cm^2]					
4.830	7	1.86	2.41	8.25[-1]	1.28	1.21[2]	2.15[2]
5.164	8	1.65	2.22	4.53[-1]	7.22[-1]	1.17[2]	2.17[2]
5.477	9	1.45	2.03	2.85[-1]	4.66[-1]	1.10[2]	2.15[2]
5.774	10	1.28	1.86	1.96[-1]	3.36[-1]	1.03[2]	2.11[2]
6.325	12	1.03	1.62	1.21[-1]	2.39[-1]	8.94[1]	2.02[2]
7.071	15	7.85[-1]	1.38	1.36[-1]	2.55[-1]	7.38[1]	1.87[2]
7.746	18	6.27[-1]	1.21	1.67[-1]	2.76[-1]	6.17[1]	1.71[2]

Table III. Calculated cross sections for the production of the $2s2p\,^3P$ and $2s2p\,^1P$ states in collisions of mixed-state C $^{4+}(1s^2,^{3,1}S)$ ion beams with He as a function of projectile energy E_p. Listed from left to right are the projectile velocity V_p and energy E_p, the 3eAOCC partial cross section for $M_L = 0$, $\sigma(M_L = 0)$, and the total production cross sections $\sigma^{tot} = \sigma(M_L = 0) + 2\sigma(M_L = 1)$. An uncertainty of about 15% is assigned to all computed cross sections (see text). The notation 4.31[-1] stands for 4.31×10^{-1}.

[a] $V_p(\text{a.u.}) \approx 2\sqrt{10\,E_p(\text{MeV})/M_p(\text{u})}$.

[b] From the$1s2s\,^3S$initial beam component the partial cross sections $\sigma(M_L)$ for the production of the $2s2p\,^3P$} are the mean of the two contributions from the doublet and quartet total spin of the collision partners $\mathbf{S}_{\text{tot}}$, i.e. $\sigma[^3S](M_L) = 0.5\sigma[^3S](M_L, \mathbf{S}_{\text{tot}} = 3/2) + 0.5\sigma[^3S](M_L, \mathbf{S}_{\text{tot}} = 1/2)$, when using a one-electron model for the He target (see text).

doi.org/10.32388/C8JRSC

		$O^{6+}(1s^2, 1s2s\,^{3,1}S) + He \rightarrow O^{6+}(2s2p\,^{3,1}P) + He(All)$					
V_p	E_p	$O^{6+}(1s^2)$		$O^{6+}(1s2s\,^3S)$		$O^{6+}(1s2s\,^1S)$	
		$\sigma(M_L=0)$	σ^{tot}	$\sigma(M_L=0)$	σ^{tot}	$\sigma(M_L=0)$	σ^{tot}
(a.u.)	(MeV)	[$\times 10^{-21}$ cm^2]					
		$2s2p\,^3P$:					
1.826	1.33	-	3.88[-4]	-	3.14	-	4.36[-2]
2.582	2.67	-	1.69[-2]	-	3.27	-	1.49
3.162	4.00	-	5.36[-2]	-	1.32[1]	-	2.63
3.652	5.33	-	5.88[-2]	-	2.19[1]	-	2.78
4.082	6.67	-	4.02[-2]	-	2.91[1]	-	2.36
4.472	8	1.91[-2]	2.22[-2]	2.51[1]	3.74[1]	1.59	2.06
5.000	10	8.11[-3]	9.63[-3]	3.39[1]	5.37[1]	1.35	1.75
5.244	11	5.42[-3]	6.42[-3]	3.87[1]	6.26[1]	1.14	1.49
5.477	12	3.67[-3]	4.29[-3]	4.32[1]	7.13[1]	8.97[-1]	1.20
5.916	14	2.09[-3]	2.35[-3]	5.01[1]	8.60[1]	4.94[-1]	7.26[-1]
6.325	16	1.79[-3]	1.98[-3]	5.38[1]	9.58[1]	2.55[-1]	4.29[-1]
6.709	18	1.76[-3]	1.94[-3]	5.50[1]	1.01[2]	1.51[-1]	2.82[-1]
7.071	20	1.68[-3]	1.89[-3]	5.29[1]	1.01[2]	1.17[-1]	2.18[-1]
7.746	24	1.42[-3]	1.69[-3]	5.11[1]	1.04[2]	7.98[-2]	1.70[-1]
		$2s2p\,^1P$:					
1.826	1.33	-	6.83[-4]	-	9.75[-2]	-	3.86[-1]
2.582	2.67	-	1.04[-2]	-	7.71[-1]	-	3.01
3.162	4.00	-	1.40[-1]	-	2.93	-	1.39[1]
3.652	5.33	-	3.40[-1]	-	3.70	-	2.37[1]
4.082	6.67	-	4.45[-1]	-	3.12	-	3.09[1]
4.472	8	4.01[-1]	4.69[-1]	1.97	2.63	2.61[1]	3.86[1]
5.000	10	4.08[-1]	4.96[-1]	1.47	1.99	3.53[1]	5.51[1]
5.244	11	4.23[-1]	5.21[-1]	1.17	1.60	4.03[1]	6.42[1]

doi.org/10.32388/C8JRSC

		$O^{6+}(1s^2, 1s2s\,^{3,1}S) + He \rightarrow O^{6+}(2s2p\,^{3,1}P) + He(All)$					
V_p	E_p	$O^{6+}(1s^2)$		$O^{6+}(1s2s\,^3S)$		$O^{6+}(1s2s\,^1S)$	
		$\sigma(M_L=0)$	σ^{tot}	$\sigma(M_L=0)$	σ^{tot}	$\sigma(M_L=0)$	σ^{tot}
(a.u.)	**(MeV)**	**[$\times 10^{-21}$ cm^2]**					
5.477	12	4.40[-1]	5.47[-1]	8.89[-1]	1.25	4.50[1]	7.31[1]
5.916	14	4.54[-1]	5.75[-1]	4.76[-1]	7.21[-1]	5.20[1]	8.77[1]
6.325	16	4.39[-1]	5.66[-1]	2.49[-1]	4.24[-1]	5.56[1]	9.73[1]
6.709	18	4.06[-1]	5.32[-1]	1.49[-1]	2.79[-1]	5.67[1]	1.03[2]
7.071	20	3.67[-1]	4.88[-1]	1.13[-1]	2.15[-1]	5.61[1]	1.05[2]
7.746	24	2.23[-1]	3.30[-1]	9.66[-2]	1.69[-1]	5.27[1]	1.05[2]

Table IV. Same as Table III, but for oxygen. Entries indicated by — means no result was calculated.

doi.org/10.32388/C8JRSC

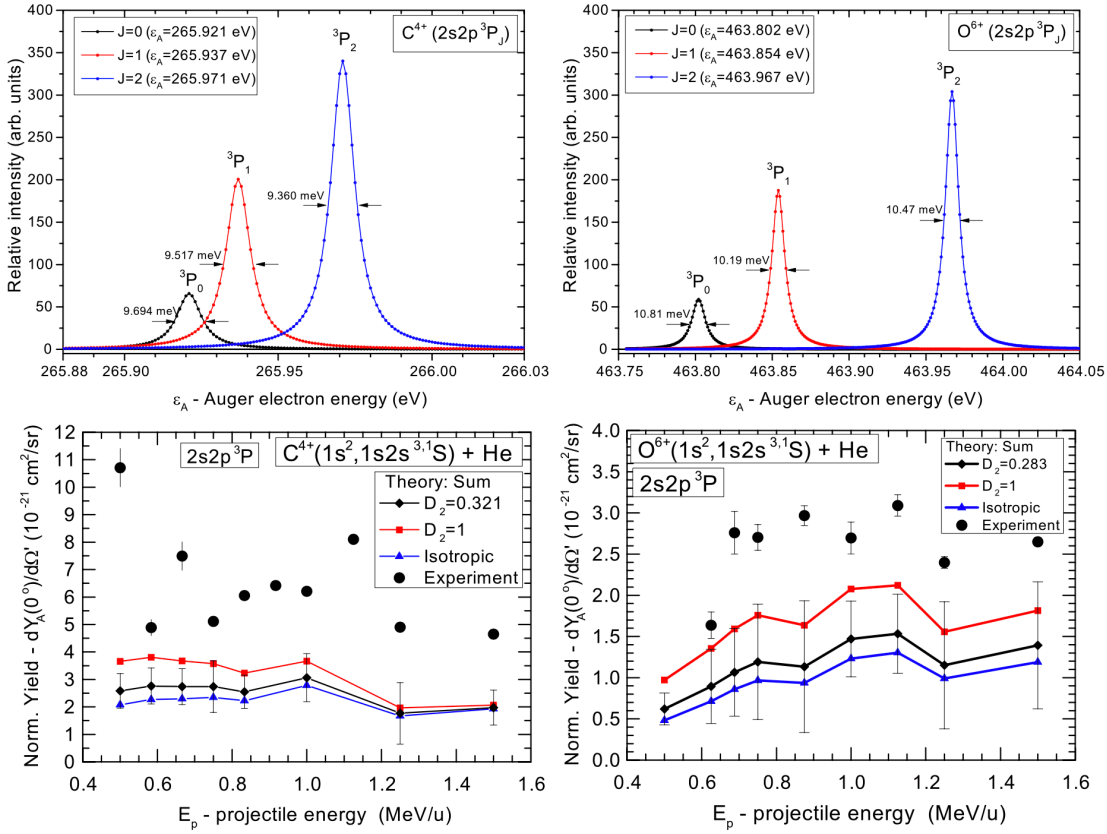

Figure 13. Top: Fine structure of carbon (left) and oxygen (right) $2s2p\,^3P_{0,1,2}$ resonances (Lorentzians) using parameters from TableVI leads to a dealignment coefficient of $D_2 = 0.321$ for carbon and $D_2 = 0.283$ for oxygen. Bottom: Comparison of the three different calculated normalized yields to the experimental data. The degree of relative overlap of the three J levels (top) affects the value of the D_2 dealignment coefficient calculated using Eq. (C1). A value of $D_2 = 1$ corresponds to maximum overlap or minimal fine structure level separation. A value of $D_2 = 0$ corresponds to isotropy.

Appendix B. Correction of the $C^{4+}(2s2p\,^1P)$ normalized yields due to SEC contribution from $(1s2s\,^3S)3d\,^2D$

The $(1s2s\,^3S)3d\,^2D$ contribution were estimated from our $(1s2s\,^3S)3d\,^4D$ SEC cross sections (they were assumed to be roughly equal - see Table VII in Ref.[19]) calculated in a one-electron AOCC (1eAOCC) treatment since our SEC 3eAOCC calculations included only $l = 0$ and $l = 1$ orbitals[19]. Furthermore, an isotropic emission was assumed from this state. These 1eAOCC SEC cross sections $\sigma[(1s2s\,^3S)3d\,^2D]$ were also multiplied by 2 to further account for the two He electrons, a correction that was shown in previous work[19] to be in principle justifiable in the case of SEC. Their contribution to the $2s2p\,^1P$ normalized yields were thus computed as $2f[^3S]\bar{\xi}[(1s2s\,^3S)3d\,^2D]\sigma[(1s2s\,^3S)3d\,^2D]/(4\pi)$ with $\bar{\xi}[(1s2s\,^3S)3d\,^2D] = 0.86$[70]. They are depicted as Gaussians with the corresponding area in Fig. 3 and were subtracted and shown as the dashed line in Figs. 11 (top) and 12 (top).

doi.org/10.32388/C8JRSC

These $(1s2s\,^3S)3d\,^2D$ results can be considered as rough estimates. Never-the-less they do seem to correctly indicate that SEC to this state drops rapidly with increasing projectile energy E_p, in agreement with the observed drop in intensity of the other $(1s2s\,^3S)3s\,^2S$ and $(1s2s\,^3S)3p\,^2P$ Auger lines seen in Fig. 3 with increasing E_p.

Appendix C. D_2 dealignment factor and effect of fine structure

The dealignment factor D_2 appearing in the Auger angular distributions [Eq. (15)] accounts for the average loss of orbital alignment into spin alignment in states having fine structure and is given by (see Eq. 20 in Ref.[58]):

$$D_2 = \sum_{J,J'=0,1,2} \frac{(2J+1)(2J'+1)}{3} \frac{\begin{Bmatrix} J & J' & 2 \\ 1 & 1 & 1 \end{Bmatrix}^2}{(1+\varepsilon_{JJ'}^2)} \tag{C1}$$

$$\varepsilon_{JJ'} = \frac{\Delta E(J,J')}{\Gamma(J,J')} \tag{C2}$$

where $\Delta E(J,J')$ and $\Gamma(J,J')$ are defined as:

$$\Delta E(J,J') = |BE[J] - BE[J']| \tag{C3}$$

$$\Gamma(J,J') = \frac{\Gamma[J] + \Gamma[J']}{2}. \tag{C4}$$

Here, $BE[J]$ and $\Gamma[J]$ are the energies and line widths of the state $2s2p\,^3P_J$ with $J = 0, 1, 2$ given in Table VI. The parameters $\varepsilon_{JJ'}$ and $\Gamma_{JJ'}$ have been computed in Table V leading to dealignment factors $D_2 = 0.321$ and 0.283, for the $2s2p\,^3P$ states of carbon and oxygen, respectively.

J	J'	$\Delta E(J,J')$[a]	$\Gamma(J,J')$[b]	$\varepsilon_{J,J'}$[c]	D_2[d]
		(meV)	**(meV)**		
$C^{4+}(2s2p^3\ ^5P)$					
0	1	15.5	9.606	1.62	
1	2	34.3	9.439	3.64	
0	2	49.8	9.528	5.24	
					0.321
$O^{6+}(2s2p^3\ ^5P)$					
0	1	51.73	10.50	4.92	
1	2	112.9	10.33	10.9	
0	2	164.6	10.64	15.5	
					0.283

Table V. Fine structure parameters used in the computation of the dealignment factor D_2 for the carbon and oxygen $2s2p^3P$ states.

[a] Fine structure energy splitting $\Delta E(J,J') = |BE[J] - BE[J']|$ with binding energies $BE[J]$ from Table VI.

[b] Mean adjacent widths[57], $\Gamma(J,J') \equiv (\Gamma[J] + \Gamma[J'])/2$ with natural widths $\Gamma[J]$ from Table VI.

[c] Mehlhorn and Taulbjerg[58] overlap parameter

$\varepsilon_{J,J'} \equiv \Delta E(J,J')/\Gamma(J,J').\}$

[d] Mehlhorn and Taulbjerg[58] dealignment parameter D_k, given for $k = 2$ by Eq. (C1).

State	J	$E_{\rm res}$	BE[b]	ε_A[d]	Γ[e]	A_a[e]	A_x[e]	ξ[f]
		(eV)	(eV)	(eV)	(meV)	(s^{-1})	(s^{-1})	
C^{4+}								
$2s2p\,^3P_0$	0	359.0493[a]	-224.07174[b]	265.921	9.694[g]	1.402[13][g]	7.058[11][g]	0.9521
$2s2p\,^3P_1$	1	359.0649[a]	-224.05620[b]	265.937	9.517[g]	1.375[13][g]	7.058[11][g]	0.9512
$2s2p\,^3P_2$	2	359.0992[a]	-224.02191[b]	265.971	9.360[g]	1.352[13][g]	7.059[11][g]	0.9504
$2s2p\,^3P$	mean			265.954	9.449			0.9508
O^{6+}								
$2s2p\,^3P_0$	0	-	-407.60768	463.802	10.81[h]	1.454[13][h]	1.885[12][i]	0.8852
$2s2p\,^3P_1$	1	-	-407.55595	463.854	10.19[h]	1.409[13][h]	1.381[12][i]	0.9107
$2s2p\,^3P_2$	2	-	-407.44308	463.967	10.47[h]	1.366[13][h]	2.245[12][i]	0.8589
$2s2p\,^3P$	mean			463.911	10.41[h]			0.8791

Table VI. Fine structure details of carbon and oxygen $2s2p\,^3P_J$ levels. Entries indicated by – means no result was acquired. Lorentzians with the tabulated parameters are depicted in Fig. 13.

[a] Resonance energy of the parent ion measured in the photoionization of $C^{4+}(1s2s\,^3S)$[52], i.e. $\gamma + C^{4+}(1s2s\,^3S) \rightarrow C^{4+}(2s2p\,^3P) \rightarrow C^{5+}(1s) + e^-_A$.

[b] Absolute binding energy computed from $E_{\rm res}$ as: $BE[J] = BE(^3S) + E_{\rm res}[J]$, where $BE(^3S) = -583.12107$ eV is the binding energy of $C^{4+}(1s2s\,^3S)$ (given as $-21.430284 \cdot 27.21014177$ eV in Table I[52]), slightly different from the NIST value given in our Table II.

[c] Absolute binding energy computed in eV from energies E(au) in Table IV of Zaytsev et al.[71] using 1 au = 27.21014177.

[d] Auger energy, $\varepsilon_A[J] = BE(1s) - BE[J]$, where $BE(1s)$ is the binding energy of the $(1s)$ configuration (see Table II). Center-of-gravity Auger energy computed as $\bar{\varepsilon}_A = \sum_J (2J+1)\varepsilon_A[J] / \sum_J (2J+1)$.

[e] $\Gamma[J]$ natural line width, A_a Auger and A_x radiative rates. Mean total width computed as $\bar{\Gamma} = \sum_J (2J+1)\Gamma[J] / \sum_J (2J+1)$.

[f] Auger yield $\xi[J]$. Mean Auger yield computed as $\bar{\xi} = \sum_J (2J+1)\xi[J] / \sum_J (2J+1)$.

[g] Müller et al. [52] Table I using complex rotation (CR) andmany-body perturbation theory (MBPT).

[h] Zaytsev et al. [71] Table IV using the complex-scaled configuration-interaction approach within the framework of the Dirac-Coulomb-Breit Hamiltonian.

[i] Manai et al.[72] using AMBiT code[73] (Particle–hole configuration interaction with many-body perturbation theory (CI+MBPT) for fully relativistic calculations of atomic energy levels).

Appendix D. Normalized Auger yields - Theory and Experiment

In Tables VII and VIII the determined fractional beam components and the thereupon computed normalized Auger yields are compared to the experimental yields.

$C^{4+}(1s^2, 1s2s\,^{3,1}S) + He \rightarrow C^{4+}(2s2p\,^{3,1}P) + He(All)$									0° **Normalized Auger yields**			
						Ion beam fractions[a]			**Theory**[b] **-** $\frac{dY_A^{tot}}{d\Omega'}(\theta = 0^\circ)$			**Exp.**
V_p	E_p		**Stripping**[c]	Δt_0[d]	$\alpha^{[1]}$	$f[1s^2]$[e]	$f[^3S]$[f]	$f[^1S]$[g]	**Isotropic**	D_2 **=1**	D_2 **=0.321**	$\frac{dY_A^{exp}}{d\Omega'}$
(a.u.)	**(MeV)**	**(MeV/u)**	**Method**	**[$\times 10^{-6}$ s]**	**(Eq. 10)**	**(%)**			**[$\times 10^{-21}$ cm^2/sr]**			
									$2s2p\,^3P$ ($\bar{\xi} = 0.951$[g]):			
4.472	6	0.500	GTS-FPS	1.287	0.2181	84.2(2.6)	13.0(2.5)	2.83(55)	2.07(51)	3.66(89)	2.58(63)	10.71(70)
4.839	7	0.583	(GTS-FPS)	1.191	0.2250	83.6(2.5)	13.4(2.5)	3.01(56)	2.27(54)	3.81(91)	2.76(66)	4.89(30)
5.164	8	0.667	(GTS-FPS)	1.114	0.2308	83.5(2.5)	13.4(2.5)	3.09(57)	2.30(55)	3.68(88)	2.74(65)	7.49(52)
5.477	9	0.750	GTS-FPS	1.051	0.2357	83.0(4.4)	13.8(4.3)	3.25(1.01)	2.34(81)	3.57(1.2)	2.74(94)	5.11(12)
5.774	10	0.833	(GTS-FPS)	0.997	0.2400	83.4(2.6)	13.4(2.5)	3.21(60)	2.23(53)	3.23(77)	2.55(61)	6.05(13)
6.055	11	0.917	(FTS)	2.003	0.1722	83.0(4.2)	14.5(4.1)	2.50(71)	-	-	-	6.41(5)
6.325	12	1.00	FTS	1.918	0.1771	79.3(4.3)	17.6(4.3)	3.11(76)	2.78(79)	3.67(1.1)	3.06(88)	6.21(5)
6.708	13.5	1.125	(FTS)	1.808	0.1836	82.8(4.2)	14.5(4.1)	2.67(76)	-	-	-	8.10(6)
7.071	15	1.250	FTS	1.716	0.1893	86.3(7.2)	11.5(7.1)	2.18(1.34)	1.67(1.06)	1.97(1.25)	1.77(38)	4.91(4)
7.745	18	1.500	(FTS)	1.566	0.1989	82.6(4.2)	14.5(4.1)	2.89(82)	1.93(62)	2.06(66)	1.97(64)	4.62(3)
									$2s2p\,^1P$ ($\xi = 0.9948$[h]):			
4.472	6	0.500	GTS-FPS	1.287	0.2181	84.2(2.6)	13.0(2.5)	2.83(55)	0.65(12)	1.27(21)	-	12.35(72)
4.839	7	0.583	(GTS-FPS)	1.191	0.2250	83.6(2.5)	13.4(2.5)	3.01(56)	0.69(12)	1.26(21)	-	3.12(27)
5.164	8	0.667	(GTS-FPS)	1.114	0.2308	83.5(2.5)	13.4(2.5)	3.09(57)	0.69(13)	1.20(21)	-	5.32(51)
5.477	9	0.750	GTS-FPS	1.051	0.2357	83.0(4.4)	13.8(4.3)	3.25(1.01)	0.69(19)	1.14(30)	-	2.29(12)
5.774	10	0.833	(GTS-FPS)	0.997	0.2400	83.4(2.6)	13.4(2.5)	3.21(60)	0.66(13)	1.04(19)	-	1.57(11)
6.055	11	0.917	(FTS)	2.003	0.1722	83.0(4.2)	14.5(4.1)	2.50(71)	-	-	-	1.23(06)
6.325	12	1.00	FTS	1.918	0.1771	79.3(4.3)	17.6(4.3)	3.11(76)	0.60(14)	0.859(190)	-	1.13(04)
6.708	13.5	1.125	(FTS)	1.808	0.1836	82.8(4.2)	14.5(4.1)	2.67(76)	-	-	-	1.18(04)
7.071	15	1.250	FTS	1.716	0.1893	86.3(7.2)	11.5(7.1)	2.18(1.34)	0.42(20)	0.545(240)	-	0.675(26)
7.745	18	1.500	(FTS)	1.566	0.1989	82.6(4.2)	14.5(4.1)	2.89(82)	0.47(13)	0.545(140)	-	0.460(20)

doi.org/10.32388/C8JRSC

Table VII. Theoretical and experimental results for the production of the $2s2p\,^3P$ and $2s2p\,^1P$ states in collisions of mixed-state $C^{4+}(1s^2,{}^{3,1}S)$ ion beams with He as a function of projectile energy E_p. Listed from left to right are the projectile velocity V_p and energy E_p, the ion beam stripper combinations used in the measurements (see Sec. II for explanations), the fractional composition of the three ion beam $f[1s^2]$, $f[^3S]$, $f[^1S]$ (for $i=1$), the parameter α (see Eq. (10)), the sum of the 0° normalized yield contributions from each of component $dY_A^{\rm tot}/d\Omega'$ (see Eq. (21)) and the experimentally determined 0° normalized Auger electron yields, $dY_A^{\rm exp}/d\Omega'$, respectively. Uncertainties in $dY_A^{\rm exp}/d\Omega'$ include just the statistical error, while uncertainties in the $dY_A^{\rm tot}/d\Omega'$ include both the computational uncertainty of ~15% and the listed experimental uncertainties in the ion beam fractions added in quadrature. Entries indicated by $-$ mean no result was calculated.

[a] Both $2s2p\,^3P$ and $2s2p\,^1P$ Auger lines were measured in the same spectrum so ion beam conditions were the same for both.

[b] Normalized yields, $\frac{dY_A}{d\Omega'}^{\rm tot}$, given by Eq. (21) for each of the three conditions expressed by Eq. (20) (isotropic), Eq. (18) ($D_2=1$) and Eq. (18) ($D_2=0.321$). For the $2s2p\,^1P$, only $D_2=1$ is possible since there is no fine structure in this state.}

[c] GTS: gas terminal stripper, GPS: gas post-stripper, FTS: foil terminal stripper, FPS: Foil post-stripper. Parentheses [e.g. (FTS)] indicate that the ion beam fractions for this E_p energy were interpolated from the measured values (no parentheses) which were experimentally determined using the ``two-spectra'' measuring technique[9][23].

[d] Time-of-flight of ion from last post-stripper to the target - see Eq. (19)} in supplement of Ref.[8].

[e] Ground state fraction $f[1s^2]=1-f[^3S]-f[^1S]$ with uncertainty $\Delta f[1s^2]=\sqrt{(\Delta f[^3S])^2+(\Delta f[^1S])^2}$.

[f] $1s2s\,^3S$ metastable fraction, $f[^3S]$, with an uncertainty $\Delta f[^3S]$ determined from the statistical uncertainties [see Eq. (22) in supplement of Ref.[8]] in the values of the experimentally determined ratios p and d defined in Eq. (9).

[g] $1s2s\,^1S$ metastable fraction, $f[^1S]$, determined from $f[^3S]$ according to Eq. (7) for $\beta^{[i]}=0$ with an uncertainty $\Delta f[^1S]=\alpha\,\Delta f[^3S]$.}}

[h] Mean Auger yield $\bar{\xi}$ computed from values given in Müller *et al.*[52].

[i] Auger yield $\xi=1-K$ computed from values of $K=0.00524$, the radiative branching ratio given in Goryaev *et al.* [74]. A similar value of $K=0.0052$ is also given by van der Hart and Hansen[53].

$O^{6+}(1s^2, 1s2s\,^{3,1}S) + He \rightarrow O^{6+}(2s2p\,^{3,1}P) + He(All)$									0° **Normalized Auger yields**			
						Ion beam fractions[a]			**Theory**[b]- $\frac{dY_A^{tot}}{d\Omega'}(\theta = 0^\circ)$			**Exp.**
V_p	E_p		**Stripping**[c]	Δt_0[d]	α	$f[1s^2]$[e]	$f[^3S]$[f]	$f[^1S]$[g]	**Isotropic**	D_2 **=1**	D_2 **=0.283**	$\frac{dY_A^{exp}}{d\Omega'}$
(a.u.)	**(MeV)**	**(MeV/u)**	**Method**	**[$\times 10^{-6}$ s]**	**(Eq. 10)**	**(%)**			**[$\times 10^{-21}$ cm^2/sr]**			
									$2s2p\,^3P$ ($\bar{\xi} = 0.8504$[h]):			
4.472	8	0.500	(GTS-FPS)	1.287	0.0171	80.7(5.2)	19.0(5.2)	0.33(09)	0.48(15)	0.97(30)	0.62(19)	-
5.000	10	0.625	FTS-FPS	1.151	0.0234	79.9(9.4)	19.6(9.4)	0.46(22)	0.71(36)	1.35(68)	0.89(45)	1.64(16)
5.244	11	0.688	GTS-FPS	1.097	0.0265	79.2(9.7)	20.3(9.7)	0.54(26)	0.86(43)	1.59(80)	1.07(53)	2.76(26)
5.477	12	0.750	GTS-FPS	1.051	0.0295	79.4(11.4)	20.0(11.4)	0.59(34)	0.97(57)	1.76(1.03)	1.19(70)	2.70(16)
5.701	13	0.813	(GTS-FPS)	1.009	0.0325	80.4(5.2)	19.0(5.2)	0.62(17)	-	-	-	3.99(17)
5.916	14	0.875	FTS-FPS	0.9728	0.0353	83.4(11.1)	16.1(11.1)	0.57(39)	0.94(66)	1.64(1.15)	1.13(80)	2.97(12)
6.124	15	0.938	(FTS-FPS)	0.9398	0.0381	80.3(5.2)	19.0(5.2)	0.73(20)	-	-	-	4.50(21)
6.325	16	1.000	(GTS-FPS)	0.9099	0.0409	80.2(5.2)	19.0(5.2)	0.78(21)	1.23(38)	2.07(65)	1.47(46)	2.70(19)
6.708	18	1.125	(GTS-FPS)	0.8579	0.0461	80.1(5.2)	19.0(5.2)	0.88(24)	1.30(41)	2.12(66)	1.53(77)	3.09(13)
7.071	20	1.250	FTS	1.652	0.0074	85.4(9.5)	14.5(9.5)	0.11(07)	0.99(66)	1.56(1.04)	1.15(77)	2.40(07)
7.416	22	1.375	(GTS-FPS)	0.7430	0.0600	79.9(5.2)	19.0(5.2)	1.14(31)	-	-	-	5.40(21)
7.745	24	1.500	FTS	1.581	0.0087	82.3(9.3)	17.5(9.3)	0.15(08)	1.19(66)	1.82(1.00)	1.39(77)	2.65(05)
									$2s2p\,^1P$ ($\xi = 0.9848$[h]):			
4.472	8	0.500	(GTS-FPS)	1.287	0.0171	80.7(5.2)	19.0(5.2)	0.33(09)	0.079(14)	0.184(31)		-
5.000	10	0.625	FTS-FPS	1.151	0.0234	79.9(9.4)	19.6(9.4)	0.46(22)	0.082(19)	0.183(42)		1.21(17)
5.244	11	0.688	GTS-FPS	1.097	0.0265	79.2(9.7)	20.3(9.7)	0.54(26)	0.085(20)	0.186(47)		0.94(22)
5.477	12	0.750	GTS-FPS	1.051	0.0295	79.4(11.4)	20.0(11.4)	0.59(34)	0.087(24)	0.186(47)		1.31(20)
5.701	13	0.813	(GTS-FPS)	1.009	0.0325	80.4(5.2)	19.0(5.2)	0.62(17)	-	-		0.89(15)
5.916	14	0.875	FTS-FPS	0.9728	0.0353	83.4(11.1)	16.1(11.1)	0.57(39)	0.086(29)	0.176(54)		1.29(24)
6.124	15	0.938	(FTS-FPS)	0.9398	0.0381	80.3(5.2)	19.0(5.2)	0.73(20)	-	-		0.67(25)
6.325	16	1.000	(GTS-FPS)	0.9099	0.0409	80.2(5.2)	19.0(5.2)	0.78(21)	0.101(20)	0.195(35)		1.49(18)
6.708	18	1.125	(GTS-FPS)	0.8579	0.0461	80.1(5.2)	19.0(5.2)	0.88(24)	0.108(23)	0.200(39)		0.82(12)

doi.org/10.32388/C8JRSC

$O^{6+}(1s^2, 1s2s\ ^{3,1}S) + He \rightarrow O^{6+}(2s2p^{3,1}P) + He(All)$									0° **Normalized Auger yields**			
						Ion beam fractions[a]			**Theory**[b]**-** $\frac{dY_A^{tot}}{d\Omega'}(\theta = 0^\circ)$			**Exp.**
V_p	E_p		**Stripping**[c]	Δt_0[d]	α	$f[1s^2]$[e]	$f[^3S]$[f]	$f[^1S]$[g]	**Isotropic**	D_2 **=1**	D_2 **=0.283**	$\frac{dY_A^{exp}}{d\Omega'}$
(a.u.)	**(MeV)**	**(MeV/u)**	**Method**	**[$\times 10^{-6}$ s]**	**(Eq. 10)**	**(%)**			**[$\times 10^{-21}$ cm^2/sr]**			
7.071	20	1.250	FTS	1.652	0.0074	85.4(9.5)	14.5(9.5)	0.11(07)	0.044(09)	0.092(17)		0.69(07)
7.416	22	1.375	(GTS-FPS)	0.7430	0.0600	79.9(5.2)	19.0(5.2)	1.14(31)	-	-		0.78(17)
7.745	24	1.500	FTS	1.581	0.0087	82.3(9.3)	17.5(9.3)	0.15(08)	0.036(08)	0.066(13)		0.64(05)

Table VIII. Same as Table VII, but for O^{6+}. Footnotes same as in Table VII, except where noted.

[b] Normalized yields, $\frac{dY_A}{d\Omega'}^{tot}$, given by Eq. (21) for each of the three conditions expressed by Eq. (20) (isotropic), Eq. (19) ($D_2 = 1$) and Eq. (18) ($D_2 = 0.283$). For the $2s2p\ ^1P$ only $D_2 = 1$ is possible since there is no fine structure in this state.

[h] Mean Auger yield $\bar{\xi}$ computed from values given in Goryaev *et al.*[74].

[i] Auger yield $\xi = 1 - K$ computed from values of $K = 0.0152$, the radiative branching ratio given in Goryaev *et al.* [74].

Appendix E. Carbon and Oxygen Auger line identification and energy level diagrams

For accurate spectroscopic work when dealing with Auger emission from projectiles with velocities in the MeV/u range it is important to use the special relativistic electron energy transformations from the laboratory to the projectile rest frame and back. For known Auger electron energy ε', the laboratory electron energy $\varepsilon_\pm(\theta)$ at the observation of θ is given in Doukas *et al.*[75]. Evaluating for our needs here at the $\theta = 0^\circ$ ($\theta' = 0^\circ$ or 180°) laboratory observation angle we have:

$$\varepsilon_\pm(0^\circ) = \gamma_p\varepsilon' + t_p \pm \sqrt{(1+\gamma')\varepsilon'(1+\gamma_p)t_p} \tag{E1}$$

where, in the projectile rest frame, the $(+)$ sign corresponds to forward emission ($\theta' = 0^\circ$) and the $(-)$ sign to backward emission ($\theta' = 180^\circ$). Primed quantities refer to the projectile rest frame, while unprimed to the laboratory frame. The reverse transformations are also given as:

$$\varepsilon' = \gamma_p\varepsilon_\pm(0^\circ) + t_p - \sqrt{(1+\gamma)\varepsilon_\pm(0^\circ)(1+\gamma_p)t_p} \tag{E2}$$

where the three relativistic γ-factors have the usual definitions:

$$\gamma_p \equiv 1 + \frac{t_p}{mc^2}, \quad \gamma \equiv 1 + \frac{\varepsilon}{mc^2}, \quad \gamma' \equiv 1 + \frac{\varepsilon'}{mc^2} \tag{E3}$$

with t_p, the reduced projectile energy (also known as the cusp energy), given by

$$t_p = \frac{m}{M_p} E_p \tag{E4}$$

where m and M_p are the masses of the electron and the projectile, respectively. In the limit of the relativistic γ-factors going to 1 we obtain the well-known classical results. As an example, we note that for the case of 18 MeV carbon ions ($t_p = 822.870$ eV) and a $2s2p\,^3P$ Auger energy $\varepsilon' = 265.95$ eV, the difference between the relativistic and classical laboratory energies amounts to more than 3 eV and is readily observable with high-resolution spectrometers.

	Experiment						Theory					
State	This work[a]	Rod79[b]	Mac87[c]	Mann87[d]	Kil93[e]	Calibration Values	Aln02[g]	Kar09[h]	Gor17[i]	Yer17[j]	Man22[k]	Man22[l]
$1s2s^2\ ^2S$	227.2(6)	227.6(5)	227.06(9)	227.1(2)	–	227.23(30)[f]	227.1	–	227.00	227.208	–	–
$1s2s2p\ ^4P$	229.6(5)	229.7(5)	229.639[p]	229.6(2)	–	229.64[f]	229.5	–	229.80	229.695	–	–
$1s2s2p\ ^2P_-$	235.5(6)	235.5(5)	235.40(4)	235.5(2)	234.3(1)	235.44(20)[f]	235.3	–	235.41	235.572	–	–
$1s2s2p\ ^2P_+$	238.8(6)	238.9(5)	238.92(4)	238.8(2)	237.8(3)	238.86(20)[f]	239.0	–	238.97	239.024	–	–
$1s2p^2\ ^2D$	242.2(6)	242.2(6)	241.98(4)	242.1(2)	241.4(1)	242.15(20)[f]	242.0	–	242.18	242.099	–	–
$2s^2\ ^1S$	264.4(6)	–	–	–	–	–	264.2	264.457	264.30	264.45[m]	263.936	264.417
$2s2p\ ^3P$	265.9(6)	–	–	–	–	265.954(1)[n]	265.7	–	265.94	266.02[m]	265.837	265.962
$(1s2s\ ^3S)3s\ ^2S$	270.6(6)	–	270.70(15)	270.7(2)	–	–	271.5	–	270.57	–	–	–
$(1s2s\ ^3S)3p\ ^2P$	271.9(6)	–	271.98(10)	271.8(2)	–	272.1[f]	272.4	–	271.50	–	–	–
$2p^2\ ^1D$	273.1(6)	–	–	–	–	–	272.4	273.157	272.99	273.27[o]	273.81	273.141
$2s2p\ ^1P$	273.8(7)	–	–	–	–	–	273.5	273.927	273.64	273.92[m]	274.289	273.741
$(1s2s\ ^3S)3d\ ^2D$	274.2(6)	–	274.29(10)	274.2(2)	–	274.1[f]	–	–	274.02	–	–	–
$2p^2\ ^1S$	–	–	–	–	–	–	–	–	283.029	281.810		
$(1s2s\ ^1S)3s\ ^2S$	274.8(6)	–	–	–	–	–	–	–	274.59	–	–	–
$(1s2s\ ^1S)3p\ ^2P$	276.9(6)	–	–	–	–	–	–	–	276.52	–	–	–
$(1s2s\ ^1S)3d\ ^2D$	278.5(6)	–	–	278.9(2)	–	278.7[f]	–	–	278.43	–	–	–

doi.org/10.32388/C8JRSC

Table IX. Carbon K-Auger energies ε_A listed in increasing energy (eV) resulting from $1s2lnl' \rightarrow 1s^2$ and $2l2l' \rightarrow 1s$ Auger transitions used in the identification of our observed Auger lines (this work). The former are used for energy calibration, while the latter are in the vicinity of the $2s2p\,^{3,1}P$ lines. There are no NIST[51] recommended values for the energy levels of these doubly excited states. Entries indicated by – means no result was acquired. The footnote in the header of each column gives the reference from which the values shown in the column were obtained, unless otherwise indicated. Experimental uncertainties as reported in the corresponding reference. For conversions to eV, we have used the NIST equivalents, 1 a.u. $= 27.211386245988(53)$ eV and $1\,cm^{-1} = 1.239842 \times 10^{-4}$ eV, unless otherwise indicated.

[a] Fitted Auger line peak energies after energy calibration of PSD channels according to the $1s2l2l'$ calibration values proposed by Bruch *et al.*[46] and listed in column seven.

[b] Rodbro *et al.* 1979[76] in 300 keV $C^+ + CH_4$.

[c] Mack 1987[77] weighted averages (Table 3) calibrated to the $1s2s2p\,^4P$ calculation of K.T. Chung[78].

[d] Mann 1987[79].

[e] Kilgus et al.1993[80] - Dielectronic Recombination (DR) measurements at the Heidelberg Test Storage Ring (TSR).

[f] Bruch *et al.* 1985[46] - Proposed calibration of carbon K-Auger energies based on the measurements by Rodbro *et al.* [76] and theory.

[g] Alnaser 2002[81] (from Tables 1 and 6) using $\varepsilon_A = Z_p^2 E_0 + Z_p E_1 + E_2$ with coefficients for each state E_0, E_1, E_2 from Rodbro *et al.*[76].

[h] Kar and Ho 2009[82] - Stabilization method: $2l2l'\ ^1L$ levels in a.u.

[i] Goryaev *et al.* 2017 [74] - MZ code with relativistic corrections: $1s2l2l'$ and $2l2l'$ levels in keV.

$\varepsilon_A(1s2snl) = \Delta E_x(1s2snl \rightarrow 1s^2 2p) + E(1s^2 2p) - E(1s^2)$,

$\varepsilon_A(2s2p) = \Delta E_x(2s2p\,^{3,1}P_J \rightarrow 1s2s\,^{3,1}S) + E(1s2s\,^{3,1}S) - E(1s)$,

where ΔE_x is the value of the x-ray transition energy given in Ref. [74] and

$E(1s^2), E(1s), E(1s2s\,^{3,1}S)$ and $E(1s^2 2p)$ the energy levels given in Table II.

[j] Yerokhin *et al.* 2017[83] - Relativistic configuration-interaction calculation of transition wavelengths. Used $hc = 1.23984198 \times 10^{-4}$ eV-cm to convert wavelength (cm) to energy (eV). See also similar, but older MCDF results by Safronova and Bruch 1994[84].

[k] Manai *et al.* 2022 [72] E_{FAC} energy levels computed with respect to the $1s^2$ ground state using the Flexible Atomic code (FAC)[85]. $\varepsilon_A(2l2l'\,^{3,1}L_J) = E_{\mathrm{FAC}}(2l2l'\,^{3,1}L_J) + E(1s^2) - E(1s)$.

[l] Manai et al. 2022 [72] E_{AMBiT} energy levels computed with respect to the $1s^2$ ground state using the AMBiT code[73] (Particle–hole configuration interaction with many-body perturbation theory (CI+MBPT) for fully relativistic calculations of atomic energy levels). $\varepsilon_A(2l2l'\,^{3,1}L_J) = E_{\mathrm{AMBiT}}(2l2l'\,^{3,1}L_J) + E(1s^2) - E(1s)$.

[m] Ho 1981[86] - complex rotation calculations as quoted in Table 4.5 of Mack 1987[87].

doi.org/10.32388/C8JRSC

[n] Müller *et al.* 2018[52] - The $2s2p\,^3P_J$ resonance energies were obtained in photoionization measurements of C^{4+} $(1s2s\,^3S)$ ions after fitting to theory from which the listed Auger energies were determined (see also Table VI). This is probably the most accurate determination to date and should be used for calibration.

[o] Peacock et al. 1973[88] - Hartree-Fock type calculations as quoted in Table 4.5 of Mack 1987[87].

[p] K.T. Chung 1984[78] - Hartree-Fock with relativistic, Breit-Pauli operator and mass-polarization corrections.

	Experiment				Theory							
State	This work[a]	Mac87[b]	Bru87[c]	Kil90[d]	Bru87[c]	Aln02[e]	Kar09[f]	Gor17[g]	Yer17[h]	Man22[i]	Man22[j]	NIST[k]
$1s2s^2\ ^2S$	412.3(7)	412.67(8)	412.7(2)	–	412.63	412.4	–	412.50	412.603	–	–	–
$1s2s2p\ ^4P$	416.4(7)	416.08	416.0(2)	–	416.02	415.5	–	416.12	415.973	–	–	416.124
$1s2s2p\ ^2P_-$	425.1(7)	424.81(8)	425.0(2)	424.9371(31)[n]	424.99	424.4	–	424.91	424.945	–	–	424.474
$1s2s2p\ ^2P_+$	428.8(7)	429.38(15)	429.6(2)	–	429.71	429.4	–	429.63	429.601	–	–	430.094
$1s2p^2\ ^2D$	434.6(7)	434.31(8)	434.4(2)	–	434.38	434.6	–	434.49	434.313	–	–	434.382
$2s^2\ ^1S$	461.5(7)	–	463(2)[l]	461.9(9)	462.3[l]	–	462.080	461.60	–	461.197	461.924	–
$2s2p^{\mathrm{m}}\ ^3P$	463.7(7)	–	466(2)[l]	463.9(1)	464.4[l]	463.3	–	463.78	–	463.677	464.002	464.029
$2p^2\ ^1D$	473.8(7)	–	471[l]	474.1(1)	474.8[l]	–	474.145	473.86	–	474.583	474.143	474.275
$2s2p^{\mathrm{m}}\ ^1P$	474.7(7)	–	477(2)[l]	476.5(12)	476.0[o]	474.1	475.230	474.79	–	475.299	475.034	475.076
$2p^2\ ^1S$	485.7(7)	–	–	485.8(1)	–	–	–	485.73	–	487.042	485.971	480.204
$(1s2s\ ^3S)3s\ ^2S$	500.3(7)	500.4(2)	–	–	500.5[l]	500.8	–	–	–	–	–	–
$(1s2s\ ^3S)3p\ ^2P$	501.8(7)	501.9(1)	–	–	502.7[l]	502.2	–	–	–	–	–	–
$(1s2s\ ^3S)3d\ ^2D$	505.5(7)	505.6(1)	–	–	506.1[l]	–	–	–	–	–	–	–
$(1s2s\ ^1S)3s\ ^2S$	–	–	–	–	506.2[l]	–	–	–	–	–	–	–
$(1s2s\ ^1S)3p\ ^2P$	–	–	–	–	509.9	–	–	–	–	–	–	–
$(1s2s\ ^1S)3d\ ^2D$	–	–	–	–	512.7[l]	–	–	–	–	–	–	–

doi.org/10.32388/C8JRSC

Table X. Same as Table IX, but for oxygen. Auger energies computed from NIST recommended energy level values are listed in the last column.}

[a] Fitted Auger line peak energies after energy calibration of PSD channels according to the values Mack 1987[77], listed in the 2nd column.

[b] Mack 1987[77] - see Table IX.

[c] Bruch *et al.* 1987[89] - Zero-degree Auger projectile spectroscopy measurements and saddle-point technique with relativistic corrections.

[d] Kilgus *et al.* 1990[45] - Dielectronic Recombination (DR) measurements at the Heidelberg Test Storage Ring (TSR).

[e] Alnaser 2002[81] - see Table IX.

[f] Kar and Ho 2009[82] - Stabilization method: $2l2l'\ ^1L$ levels in a.u.

[g] Goryaev *et al.* 2017[74] - see Table IX.

[h] Yerokhin *et al.* 2017[83] - see Table IX.

[i] Manai *et al.*[72] using FAC code - see Table IX.

[j] Manai *et al.* [72] using AMBiT code - see Table IX.

[k] $\varepsilon_A(1s2l2l') = E(1s2l2l') - E(1s^2) + E(1s^22s)$ or $\varepsilon_A(2l2l') = E(2l2l') - E(1s) + E(1s^2)$, where $E(1s2l2l')$ and $E(2l2l')$ are the given NIST energies with respect to $1s^22s$ or $1s^2$, respectively[51].

[l] Bruch *et al.* 1979[44] - 23.7° ESCA measurements and semiempirical + *ab initio* theoretical methods.

[m] See also Ho[86] - complex rotation method - which gives Auger energies of 464.25 and 475.23 eV, for $2s2p\ ^3P$ and ^1P, respectively.

[n] Togawa *et al.*[90] for the most accurate to date experimental values of $1s2s2p\ ^2P_{1/2-}$ and $1s2s2p\ ^2P_{3/2-}$ to $1s^22s$ x-ray transition energies from which we obtain a center-of-gravity Auger energy of $\bar{\varepsilon}_A[1s2s2p\ ^2P_-] = 424.9371(31)$ eV using the NIST value for the IP of $O^{5+}(1s^22s) = 138.1189(21)$ eV[91].

[o] Ahmed and Lipsky 1975[92] quoted in Bruch *et al.* 1979[44].

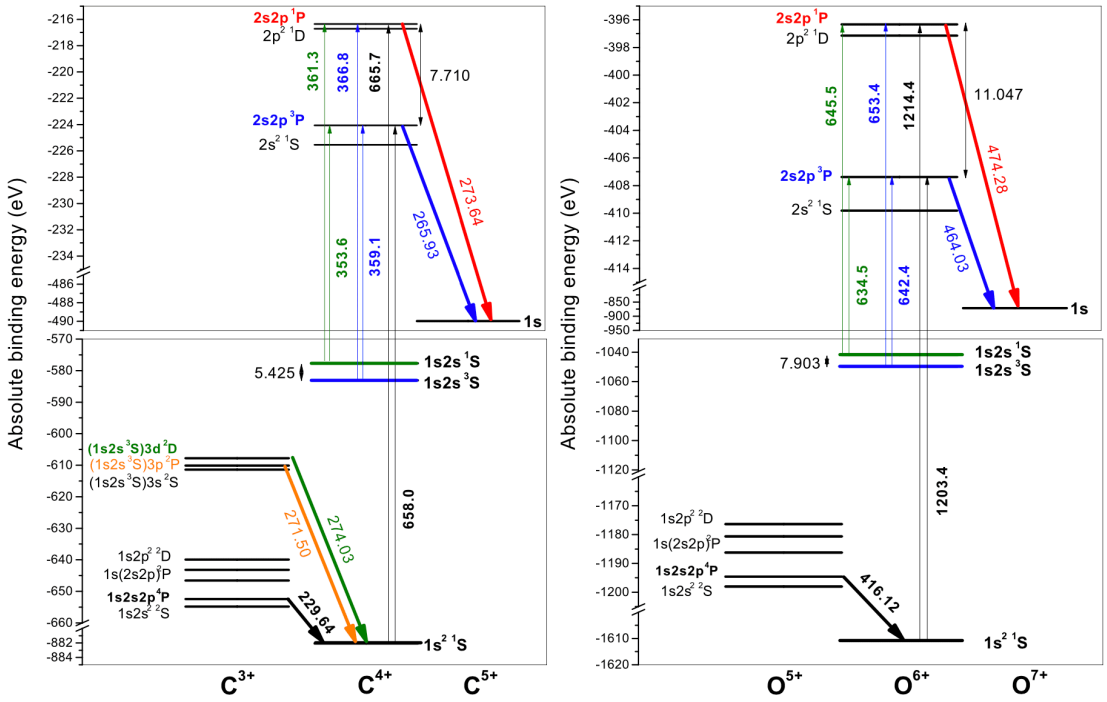

Figure 14. Absolute binding energies of relevant carbon (left) and oxygen (right) levels. Auger transitions and their energies in eV (downward arrows slanted to the right). Bottom panel (left): Black $C^{3+}(1s2s2p\,^4P)$ calibration line[46], green $C^{3+}[(1s2s\,^3S)3d\,^2D]$, orange $C^{3+}[(1s2s\,^3S)3p\,^2P]$. Top panels: Blue $(2s2p\,^3P)$ and red $(2s2p\,^1P)$ Auger transitions. The six excitation energies from each of the three initial ion beam components $1s^2$, $1s2s\,^3S$ and $1s2s\,^3S$ to the two final states $2s2p^1P$ and $2s2p^3P$ are also shown (thin upward pointing arrows). The levels $1s2s3l$ are not indicated for oxygen (bottom right) as in the case of carbon because as shown in Table X their Auger energies are quite a bit larger than the $2s2p\,^{3,1}P$ and therefore not a problem to identify as in the case of carbon.

References

1. a, b, c, d, e, f, g, h, i, j, k, l, m, n *A. Laoutaris, S. Nanos, A. Biniskos, S. Passalidis, E. P. Benis, A. Dubois, and T. J. M. Zouros, Projectile excitation to autoionizing states in swift collisions of open-shell He-like ions with helium, Phys. Rev. A 109, 032825 (2024).*
2. ^ *E. P. Benis, Fast ion-atom collisions: Electron spectroscopy of mixed-state beams, in Advances in Atomic Molecular Collisions, edited by L. C. Tribedi (Springer Nature Singapore, Singapore, 2024) pp. 71–110.*
3. a, b, c *N. Sisourat and A. Dubois, Semiclassical close-coupling approaches, in Ion-Atom Collision - The Few-Body Problem in Dynamic Systems, edited by M. Schultz (de Gruyter, Berlin/Boston, 2019) pp. 157–178.*
4. ^ *A. H. Gabriel, Dielectronic Satellite Spectra for Highly-Charged Helium-Like Ion Lines, MNRAS 160, 99 (1972).*
5. ^ *P. Beiersdorfer, Laboratory X-ray astrophysics, Annu. Rev. Astron. Astrophys. 41, 343 (2003).*

6. ^F. Delahaye, A. K. Pradhan, and C. J. Zeippen, Electron impact excitation of helium-like ions up to n = 4 levels including radiation damping, J. Phys. B 39, 3465 (2006).
7. ^W. Fritsch, Electron excitation in collisions between protons and excited helium, Phys. Lett. A 158, 227 (1991).
8. a, b, c, d, e, f, g, h, i, j, k, l, m, n, o, p, q, rT. J. M. Zouros, A. Laoutaris, S. Nanos, and E. P. Benis, Determination of the 1s2s^{3} ext{S} and 1s2s^{1} ext{S} metastable fractions in swift mixed-state He-like ion beams, J. Phys. B 10.1088/1361-6455/adb54d (2025), and Supplemental Material.
9. a, b, c, d, e, fE. P. Benis, I. Madesis, A. Laoutaris, S. Nanos, and T. J. M. Zouros, Mixed-state ionic beams: An effective tool for collision dynamics investigations, Atoms 6, 66 (2018).
10. ^E. H. Pedersen, Metastable-Atom Population of Fast, Neutral Helium Beams, Phys. Rev. Lett. 42, 440 (1979).
11. a, bT. R. Dillingham, J. Newcomb, J. Hall, P. L. Pepmiller, and P. Richard, Projectile K-Auger-electron production by bare, one-, and two-electron ions, Phys. Rev. A 29, 3029 (1984).
12. a, b, c, d, eL. H. Andersen, G. Y. Pan, H. T. Schmidt, N. R. Badnell, and M. S. Pindzola, Absolute measurements and calculations of dielectronic recombination with metastable He-like N, F, and Si ions, Phys. Rev. A 45, 7868 (1992a).
13. ^A. Dinklage, T. Lokajczyk, and H. J. Kunze, Measurement of the 2^{3} ext{S} population in a ^{4}He beam by means of laser-induced fluorescence, J. Phys. B 29, 1655 (1996).
14. a, b, cM. Zamkov, H. Aliabadi, E. P. Benis, P. Richard, H. Tawara, and T. J. M. Zouros, Energy dependence of the metastable fraction in B3+ (1s2 1S, 1s2s 3S) beams produced in collisions with thin-foil and gas targets, Phys. Rev. A 64, 052702 (2001).
15. a, b, c, dE. P. Benis, M. Zamkov, P. Richard, and T. J. M. Zouros, Technique for the determination of the 1s2s^{3} ext{S} metastable fraction in two-electron ion beams, Phys. Rev. A 65, 064701 (2002).
16. a, bI. S. Dmitriev, Y. A. Teplova, Y. A. Fainberg, and Y. A. Belkova, Formation of metastable states of light ions in ion–atom collisions, Phys. Scr. 68, 383 (2003).
17. a, bM. Zamkov, H. Aliabadi, E. P. Benis, P. Richard, H. Tawara, and T. J. M. Zouros, Stripping energy dependence of B^{3+}{(1s2s ^{3}ext{S})} beam metastable fraction, American Institute of Physics 576, 149 (2001b).
18. a, b, c, d, e, fI. Madesis, A. Laoutaris, T. J. M. Zouros, E. P. Benis, J. W. Gao, and A. Dubois, Pauli Shielding and Breakdown of Spin Statistics in Multielectron Multi-Open-Shell Dynamical Atomic Systems, Phys. Rev. Lett. 124, 113401 (2020), and Supplemental Material.
19. a, b, c, d, e, f, g, h, i, j, k, l, mI. Madesis, A. Laoutaris, S. Nanos, S. Passalidis, A. Dubois, T. J. M. Zouros, and E. P. Benis, State-resolved differential cross sections of single-electron capture in swift collisions of C^{4+}{(1s2s ^{3}ext{S})} ions with gas targets, Phys. Rev. A 105, 062810 (2022).
20. a, b, c, d, eA. Laoutaris, S. Nanos, I. Madesis, S. Passalidis, E. P. Benis, A. Dubois, and T. J. M. Zouros, Coherent treatment of transfer-excitation processes in swift ion-atom collisions, Phys. Rev. A 106, 022810 (2022).
21. ^N. Stolterfoht, High resolution Auger spectroscopy in energetic ion atom collisions, Phys. Rep. 146, 315 (1987).

22. ^T. J. M. Zouros and D. H. Lee, Zero Degree Auger Electron Spectroscopy of Projectile Ions, in Accelerator-Based Atomic P hysics: Techniques and Applications, edited by S. M. Shafroth and J. C. Austin (American Institute of Physics, Woodbury, NY, 1997) Chap. 13, pp. 426–479.

23. a, b, c, d, e, f, g, hE. P. Benis and T. J. M. Zouros, Determination of the 1s2l2l' state production ratios 4Po/2P, 2D/2P and 2P+ /2P- from fast (1s2 , 1s2s 3S) mixed-state He-like ion beams in collisions with H2 targets, J. Phys. B 49, 235202 (2016).

24. a, bS. Nanos, A. Biniskos, A. Laoutaris, M. Andrianis, T. J. M. Zouros, A. Lagoyannis, and E. P. Benis, Determination of the i on beam energy width in tandem Van de Graaff accelerators via Auger projectile spectroscopy, Nucl. Instrum. Methods P hys. Res., Sect. B 541, 93 (2023).

25. ^J. R. Macdonald, P. Richard, C. L. Cocke, M. Brown, and I. A. Sellin, One- and two-electron excited states produced by ele ctron exchange, excitation, and electron capture in collisions of fluorine ions in argon gas at 34.8 MeV, Phys. Rev. Lett. 31, 684 (1973).

26. a, bF. Hopkins, R. L. Kauffman, C. W. Woods, and P. Richard, K x-ray transitions in one- and two-electron oxygen and fluo rine projectiles produced in helium, neon, and argon targets, Phys. Rev. A 9, 2413 (1974).

27. ^F. Hopkins, A. Little, and N. Cue, Inner-shell Coulomb excitation in the collisions of few-electron F with H2 and He, Phy s. Rev. A 14, 1634 (1976).

28. ^D. L. Matthews, R. J. Fortner, D. Schneider, and C. F. Moore, Evidence for nonstatistical population of configurations in Li -like neon following Cl13+ ightarrow Ne collisions, Phys. Rev. A 14, 1561 (1976a).

29. ^U. Schiebel, B. L. Doyle, J. R. Macdonald, and L. D. Ellsworth, Projectile K x rays from Si12+ ions in the 1s2s^{3} ext{S}_{1} metastable state incident on helium gas, Phys. Rev. A 16, 1089 (1977).

30. ^M. Terasawa, T. J. Gray, S. Hagmann, J. Hall, J. Newcomb, P. Pepmiller, and P. Richard, Electron capture by and electron e xcitation of two-electron fluorine ions incident on helium, Phys. Rev. A 27, 2868 (1983).

31. ^K. Reymann, K.-H. Schartner, B. Sommer, and E. Träbert, Scaling relation for total excitation cross sections of He in colli sions with highly charged ions, Phys. Rev. A 38, 2290 (1988).

32. ^K. Wohrer, A. Chetioui, J. P. Rozet, A. Jolly, F. Fernandez, C. Stephan, B. Brendles, and R. Gayet, Target nuclear charge dep endence of 1s^{2} to 1s2p and 1s^{2} to 1s3p excitation cross sections of Fe24+ projectiles in the intermediate velocity ran ge, J. Phys. B 19, 1997 (1986).

33. ^R. Ali, C. P. Bhalla, C. L. Cocke, M. Schulz, and M. Stockli, Dielectronic recombination on and electron-impact excitation of heliumlike argon, Phys. Rev. A 44, 223 (1991).

34. ^M. Chabot, K. Wohrer, A. Chetioui, J. P. Rozet, A. Touati, D. Vernhet, M. F. Politis, C. Stephan, J. P. Grandin, A. Macias, F. M artin, A. Riera, J. L. Sanz, and R. Gayet, New investigation of saturation effect in ion-atom excitation, J. Phys. B 27, 111 (19 94).

35. ^L. Adoui, D. Vernhet, K. Wohrer, J. Plante, A. Chetioui, J. Rozet, I. Despiney, C. Stephan, A. Touati, J. Ramillon, A. Cassimi, J. Grandin, and M. Cornille, Excitation of Ar16+ projectiles in intermediate velocity collisions with neutrals, Nucl. Instrum. Methods Phys. Res., Sect. B 98, 312 (1995).

36. ^D. L. Matthews, R. J. Fortner, and G. Bissinger, Collisional quenching of metastable x-ray-emitting states in a fast beam of He-like fluorine, Phys. Rev. Lett. 36, 664 (1976b).

37. ^S. Zuccatti, R. Bruch, and J. Rissler, Excitation cross sections of Li^{+}(1snl) ^{3}ext{L}, ^{1}ext{L} states in collisions of Li + with He, Nucl. Instrum. Methods Phys. Res., Sect. B 10-11, 231 (1985).

38. ^J. Newcomb, T. R. Dillingham, J. Hall, S. L. Varghese, P. L. Pepmiller, and P. Richard, Charge-state dependence of fluorine -projectile k Auger-electron production, Phys. Rev. A 29, 106 (1984).

39. ^D. H. Lee, P. Richard, J. M. Sanders, T. J. M. Zouros, J. L. Shinpaugh, and S. L. Varghese, Electron capture and excitation st udied by state-resolved KLL Auger measurement in 0.25-2 MeV/u F^{7+} (1s^{2} ^{1}ext{S}, 1s2s ^{3}ext{S}) + H2/He coll isions, Nucl. Instrum. Methods Phys. Res., Sect. B 56-57, 99 (1991).

40. ^S. Harissopulos, M. Andrianis, M. Axiotis, A. Lagoyannis, A. G. Karydas, Z. Kotsina, A. Laoutaris, G. Apostolopoulos, A. T heodorou, T. J. M. Zouros, I. Madesis, and E. P. Benis, The Tandem Accelerator Laboratory of NCSR "Demokritos": Current status and perspectives, Eur. Phys. J. Plus 136, 617 (2021).

41. ^E. Träbert, Long-lived levels in multiply and highly charged ions, Atoms 12, 12 (2024).

42. a, bI. Madesis, A. Laoutaris, T. J. M. Zouros, S. Nanos, and E. P. Benis, Projectile electron spectroscopy and new answers to old questions: Latest results at the new atomic physics beamline in Demokritos, Athens, in State-of-the-Art Reviews on Energetic Ion-Atom and Ion-Molecule Collisions, Interdisciplinary Research on Particle Collisions and Quantitative Spec troscopy, Vol. 2, edited by D. Belkić, I. Bray, and A. Kadyrov (World Scientific, Singapore, 2019) Chap. 1, pp. 1–31.

43. ^SIS Scientific Instrument Services, SIMION version 8.1.2.20, Ringoes, NJ, see http://www.simion.com (2014).

44. a, b, cR. Bruch, D. Schneider, W. H. E. Schwarz, M. Meinhart, B. M. Johnson, and K. Taulbjerg, Projectile Auger spectra of ga s- and foil-excited oxygen ions at MeV energies, Phys. Rev. A 19, 587 (1979).

45. a, bG. Kilgus, J. Berger, P. Blatt, M. Grieser, D. Habs, B. Hochadel, E. Jaeschke, D. Krämer, R. Neumann, G. Neureither, W. Ott, D. Schwalm, M. Steck, R. Stokstad, E. Szmola, A. Wolf, R. Schuch, A. Müller, and M. Wagner, Dielectronic Recombination o f Hydrogenlike Oxygen in a Heavy-Ion Storage Ring, Phys. Rev. Lett. 64, 737 (1990).

46. a, b, c, dR. Bruch, K. T. Chung, W. L. Luken, and J. C. Culberson, Recalibration of the KLL Auger spectrum of carbon, Phys. R ev. A 31, 310 (1985).

47. ^N. Sisourat, I. Pilskog, and A. Dubois, Non perturbative treatment of multielectron processes in ion-molecule scattering: Application to He2+-H2 collisions, Phys. Rev. A 84, 052722 (2011).

48. ^J. W. Gao, Y. Wu, J. G. Wang, N. Sisourat, and A. Dubois, State-selective electron transfer in He+ + He collisions at interme diate energies, Phys. Rev. A 97, 052709 (2018).

49. ^A. Igarashi and D. Kato, Cross sections in He+ + He collision at intermediate energies, Eur. Phys. J. D 78, 79 (2024).

50. ^I. Madesis, Investigation of electron capture in swift C^{4+} (1s2s ^{3}ext{S}) collisions with gas targets using a zero-de gree Auger projectile spectroscopy apparatus built with the L45 beam line at the "Demokritos" 5.5 MV tandem accelerat or, Ph.D. thesis, University of Crete (2021), unpublished.

51. a, b, c, dA. Kramida, Cowan code: 50 years of growing impact on atomic physics, Atoms 7, 64 (2019).

52. a, b, c, d, e, f A. Müller, E. Lindroth, S. Bari, A. Borovik, P.-M. Hillenbrand, K. Holste, P. Indelicato, A. L. D. Kilcoyne, S. Klumpp, M. Martins, J. Viefhaus, P. Wilhelm, and S. Schippers, Photoionization of metastable heliumlike C^{4+} (1s2s ^{3}ext{S}_{1}) ions: Precision study of intermediate doubly excited states, Phys. Rev. A 98, 033416 (2018).

53. a, b H. W. van der Hart and J. E. Hansen, Competition between radiative and non-radiative decay for doubly excited 2lnl' and 3lnl' states in C4+, J. Phys. B 26, 641 (1993).

54. ^ M. H. Chen, Effect of intermediate coupling on angular distribution of Auger electrons, Phys. Rev. A 45, 1684 (1992).

55. ^ A. Surzhykov, U. D. Jentschura, T. Stöhlker, A. Gumberidze, and S. Fritzsche, Alignment of heavy few-electron ions follo wing excitation by relativistic Coulomb collisions, Phys. Rev. A 77, 042722 (2008).

56. ^ S. Fritzsche, A. Surzhykov, A. Gumberidze, and T. Stöhlker, Electron emission from highly charged ions: Signatures of m agnetic interactions and retardation in strong fields, New J. Phys. 14, 083018 (2012).

57. a, b N. M. Kabachnik, J. Tulkki, H. Aksela, and S. Ricz, Coherence and correlation in the anisotropy of Ne KL-LLL satellite Auger decay, Phys. Rev. A 49, 4653 (1994).

58. a, b, c, d, e, f, g W. Mehlhorn and K. Taulbjerg, Angular distribution of electrons from autoionising states with unresolved fi ne structure, J. Phys. B 13, 445 (1980).

59. ^ T. J. M. Zouros, D. H. Lee, P. Richard, J. M. Sanders, J. L. Shinpaugh, S. L. Varghese, K. R. Karim, and C. P. Bhalla, State-sele ctive observation of Resonance Transfer Excitation (RTE) in collisions of F6+ with He and H2 targets, Phys. Rev. A 40, 62 46 (1989a).

60. a, b, c T. J. M. Zouros, D. H. Lee, and P. Richard, Projectile 1s ightarrow2p Excitation Due to Electron-Electron Interaction in Collisions of O5+ and F6+ Ions with H2 and He Targets, Phys. Rev. Lett. 62, 2261 (1989b).

61. ^ R. E. Olson and F. T. Smith, Effect of long-range forces in near-resonant charge transfer: Application to He+ + K, Rb, and Cs, Phys. Rev. A 7, 1529 (1973).

62. ^ R. W. McCullough, T. V. Goffe, and H. B. Gilbody, Formation of fast metastable helium atoms in electron capture by He+ ions in alkali-metal vapours, J. Phys. B 11, 2333 (1978).

63. ^ D. H. Lee, T. J. M. Zouros, J. M. Sanders, P. Richard, J. M. Anthony, Y. D. Wang, and J. H. McGuire, K-shell ionization of O4+ and C2+ ions in fast collisions with H2 and He gas targets, Phys. Rev. A 46, 1374 (1992).

64. ^ J. Rzadkiewicz, T. St öhlker, D. Bana ́s, H. F. Beyer, F. Bosch, C. Brandau, C. Z. Dong, S. Fritzsche, A. Gojska, A. Gumberidz e, S. Hagmann, D. C. Ionescu, C. Kozhuharov, T. Nandi, R. Reuschl, D. Sierpowski, U. Spillmann, A. Surzhykov, S. Tashenov, M. Trassinelli, and S. Trotsenko, Selective population of the [1s2s] 1S0 and [1s2s] 3S1 states of He-like uranium, Phys. Rev. A 74, 012511 (2006).

65. ^ X. Zhu, S. Zhang, Y. Gao, D. Guo, J. Xu, R. Zhang, D. Zhao, K. Lin, X. Zhu, D. Xing, S. Cui, S. Passalidis, A. Dubois, and X. Ma, Direct evidence of breakdown of spin statistics in ion-atom charge exchange collisions, Phys. Rev. Lett. 133, 173002 (202 4).

66. ^ T. J. M. Zouros, Excitation and ionization in fast ion-atom collisions due to projectile electron–target electron interactio ns, in Applications of Particle and Laser Beams in Materials Technology, Vol. 283, edited by P. Misailides, NATO Advance

d Study Institute Series E: Applied Sciences (Kluwer Academic, Netherlands, 1995) pp. 37–52.

67. ^*T. J. M. Zouros, Projectile-Electron - Target-Electron Interactions: Exposing the Dynamic Role of Electrons in Fast Ion-A tom Collisions, Comm. At. Mol. Phys. 32, 291 (1996).*

68. a, b*A. Gumberidze, D. B. Thorn, A. Surzhykov, C. J. Fontes, B. Najjari, A. Voitkiv, S. Fritzsche, D. Banaś, H. F. Beyer, W. Chen, R. E. Grisenti, S. Hagmann, R. Hess, P.-M. Hillenbrand, P. Indelicato, C. Kozhuharov, M. Lestinsky, R. Märtin, N. Petridis, R. V. Popov, R. Schuch, U. Spillmann, S. Tashenov, S. Trotsenko, A. Warczak, G. Weber, W. Wen, D. F. A. Winters, N. Winters, Z. Yin, and T. Stöhlker, Electron- and proton-impact excitation of heliumlike uranium in relativistic collisions, Phys. Rev. A 99, 032706 (2019).*

69. ^*L. H. Andersen, G.-Y. Pan, H. T. Schmidt, M. S. Pindzola, and N. R. Badnell, State-selective measurements and calculatio ns of dielectronic recombination with Li-like N4+, F6+, and Si11+ ions, Phys. Rev. A 45, 6332 (1992b).*

70. ^*E. F. Deveney, Q. C. Kessel, R. J. Fuller, M. P. Reaves, R. A. Bellantone, S. M. Shafroth, and N. Jones, Projectile Auger electro n spectra of C3+ following 12-MeV collisions with He targets, Phys. Rev. A 48, 2926 (1993).*

71. a, b*V. A. Zaytsev, I. A. Maltsev, I. I. Tupitsyn, and V. M. Shabaev, Complex-scaled relativistic configuration-interaction stud y of the LL resonances in heliumlike ions: From boron to argon, Phys. Rev. A 100, 052504 (2019).*

72. a, b, c, d, e*S. Manai, D. E. Salhi, S. B. Nasr, and H. Jelassi, Relativistic theoretical calculations of singly and doubly energy le vels, lifetimes, wavelengths, weighted oscillator strengths and radiative rates for Helium-Like Ions with Z=5-9, Results in Phys. 37, 105487 (2022).*

73. a, b*E. Kahl and J. Berengut, AMBiT: A programme for high-precision relativistic atomic structure calculations, Comp. Phy s. Com. 238, 232 (2019).*

74. a, b, c, d, e, f*F. F. Goryaev, L. A. Vainshtein, and A. M. Urnov, Atomic data for doubly-excited states 2lnl' of He-like ions and 1s2lnl' of Li-like ions with Z = 6 - 36 and n = 2,3, At. Data Nucl. Data Tables 113, 117 (2017).*

75. ^*S. Doukas, I. Madesis, A. Dimitriou, A. Laoutaris, T. J. M. Zouros, and E. P. Benis, Determination of the solid angle and res ponse function of a hemispherical spectrograph with injection lens for Auger electrons emitted from long lived projectil e states, Rev. Sci. Instrum. 86, 043111 (2015).*

76. a, b, c*M. Rødbro, R. Bruch, and P. Bisgaard, High-resolution projectile Auger spectroscopy for Li, Be, B and C excited in sin gle gas collisions I. Line energies for prompt decays, J. Phys. B 12, 2413 (1979).*

77. a, b, c*M. Mack and A. Niehaus, K-shell excited Li-like ions: Electron spectroscopy of the doublet term system, Nucl. Instru m. Methods Phys. Res., Sect. B 23, 291 (1987).*

78. a, b*K. T. Chung, Fine structures and transition wavelengths for 1s2s2p ^{4}ext{P} and 1s2p2p ^{4}ext{P} of lithiumlike io ns, Phys. Rev. A 29, 682 (1984).*

79. ^*R. Mann, High-resolution K and L Auger electron spectra induced by single- and double-electron capture from H2, He, and Xe atoms to C4+ and C5+ ions at 10–100-keV energies, Phys. Rev. A 35, 4988 (1987).*

80. ^*G. Kilgus, D. Habs, D. Schwalm, A. Wolf, R. Schuch, and N. R. Badnell, Dielectronic recombination from ground state of h eliumlike carbon ions, Phys. Rev. A 47, 4859 (1993).*

81. ^ a, b *A. S. Alnaser, Electron Correlation Leading to Double-K-Shell Vacancy Production in Li-Like Ions Colliding with Heliu m, Ph.D. thesis, Western Michigan University, Kalamazoo (2002), unpublished.*

82. ^ a, b *S. Kar and Y. K. Ho, Effect of screened Coulomb potentials on the resonance states of two-electron highly stripped ato ms using the stabilization method, J. Phys. B 42, 044007 (2009).*

83. ^ a, b *V. A. Yerokhin, A. Surzhykov, and A. Müller, Relativistic configuration-interaction calculations of the energy levels of t he 1s^{2}2l and 1s2l2l' states in lithiumlike ions: Carbon through chlorine, Phys. Rev. A 96, 042505 (2017); Erratum Phys. Rev. A 96, 069901 (2017b).*

84. ^ *U. I. Safronova and R. Bruch, Transition and Auger energies of Li-like ions (1s2lnl' configurations), Phys. Scr. 50, 45 (199 4).*

85. ^ *M. F. Gu, The flexible atomic code, Can. J. Phys. 86, 675 (2008).*

86. ^ a, b *Y. K. Ho, Complex-coordinate calculations for doubly excited states of two-electron atoms, Phys. Rev. A 23, 2137 (198 1).*

87. ^ a, b *E. M. Mack, Electron capture to autoionizing states of multiply charged ions, Ph.D. thesis, Utrecht University (1987).*

88. ^ *N. J. Peacock, M. G. Hobby, and M. Galanti, Satellite spectra for helium-like ions in laser-produced plasmas, J. Phys. B 6, L298 (1973).*

89. ^ *R. Bruch, N. Stolterfoht, S. Datz, P. D. Miller, P. L. Pepmiller, Y. Yamazaki, H. F. Krause, and J. K. Swenson, High-resolution KLL Auger spectra of multiply ionized oxygen projectiles studied by zero-degree electron spectroscopy, Phys. Rev. A 35, 4 114 (1987).*

90. ^ *M. Togawa, S. Kühn, C. Shah, V. A. Zaytsev, N. S. Oreshkina, J. Buck, S. Bernitt, R. Steinbrügge, J. Seltmann, M. Hoesch, C. H. Keitel, T. Pfeifer, M. A. Leutenegger, and J. R. C. López-Urrutia, High-accuracy measurements of core-excited transitio ns in light Li-like ions, Phys. Rev. A 110, L030802 (2024).*

91. ^ *A. Kramida, Yu. Ralchenko, and J. R. and NIST ASD Team, NIST atomic spectra database (v5.11), https://physics.nist.gov/ asd (2024), Gaithersburg, MD: National Institute of Standards and Technology.*

92. ^ *M. Ahmed and L. Lipsky, Triply excited states of three-electron atomic systems, Phys. Rev. A 12, 1176 (1975).*

Declarations

Funding: No specific funding was received for this work.

Potential competing interests: No potential competing interests to declare.